**Non-canonical role of E3 ligase RIPLET in innate immunity as a co-receptor for RIG-I**

Short title: RIPLET is a co-receptor for RIG-I

One-sentence summary: RIPLET functions as a molecular glue to assemble signaling scaffolds for the antiviral innate immune receptor RIG-I.

Cristhian Cadena[1,2,3], Sadeem Ahmad[2,3], Audrey Xavier[3,4], Ji Woo Park[3,5], Seong-Wook Oh[6], Takashi Fujita[6], Fajian Hou[7] and Sun Hur[1,2,3]

[1]Program in Virology, Division of Medical Sciences

[2]Department of Biological Chemistry and Molecular Pharmacology

Harvard Medical School, Boston, MA 02115, USA

[3]Program in Cellular and Molecular Medicine

Boston Children's Hospital, MA 02115, USA

[4]Institute of Chemistry and Biochemistry, Free University of Berlin, Germany

[5]Biology Department, Boston College, Chestnut Hill, USA

[6] Laboratory of Molecular Genetics, Institute for Frontier Life and Medical Sciences, Kyoto University, Japan

[7]Shanghai Institute of Biochemistry and Cell Biology, University of Chinese Academy of Sciences, China

*correspondence: Sun.Hur@childrens.harvard.edu

**Abstract**

Ubiquitin (Ub) and its E3 ligases play diverse biological roles, from proteasomal degradation to innate immune signaling. The conventional view posits that E3 ligases function primarily through conjugating Ub to their substrate molecules. We report here that RIPLET, an essential E3 ligase in antiviral immunity, promotes the antiviral signaling activity of the viral RNA receptor RIG-I through both Ub-dependent and -independent manners. RIPLET utilizes its dimeric structure and the bivalent binding mode to preferentially recognize RIG-I pre-oligomerized on dsRNA. RIPLET can also adopt an alternative binding mode for filamentous oligomers of RIG-I assembled on longer dsRNAs, cross-bridging RIG-I filaments in both ubiquitin-dependent and -independent manners. The resultant receptor clustering leads to the formation of aggregate-like cytosolic granules and the stimulation of RIG-I-mediated antiviral signaling in a RNA-length dependent manner. These observations show the unexpected role of an E3 ligase as a co-receptor that directly participates in receptor oligomerization and ligand discrimination. This study also highlights previously unrecognized mechanisms by which an E3 ligase induces receptor clustering and signal amplification, and offers insights into the unique cellular function of membrane-less granule assembly.

**Main Text**

The innate immune receptor RIG-I recognizes RNAs from a broad range of viruses, and activates antiviral signaling pathways to produce type I and III interferons (IFNs) and other inflammatory cytokines (*1, 2*). RIG-I recognizes double-stranded RNA (dsRNA) with a 5'-triphosphate (5'ppp) or diphosphate group (*3, 4*). The RNA recognition then leads to the activation of the downstream adaptor molecule, MAVS, for antiviral signal activation (*1, 2*). Previous structural and biochemical studies have revealed a detailed picture of how RIG-I recognizes dsRNA with 5'ppp and how viral RNA binding leads to signal activation (*5-7*). In the absence of viral RNA, RIG-I is in the autorepressed state wherein the signaling domain, the N-terminal tandem CARD (2CARD), is inhibited from activating MAVS (*8*). dsRNA binding occurs via the RIG-I helicase domain and the C-terminal domain (CTD), which together bind the dsRNA end and recognize the 5'ppp (*9, 10*). While RIG-I binds to the end of dsRNA as a monomer, it assembles a filamentous oligomer on longer dsRNAs through ATP-driven translocation from the dsRNA end (*11, 12*). Regardless of the oligomeric state of RIG-I on RNA, dsRNA binding or the subsequent ATP binding was proposed to release the auto-repression of 2CARD (*8, 13*). The released 2CARD then forms a tetramer and recruits MAVS through the homotypic CARD-CARD interaction (*14, 15*). This interaction nucleates MAVS CARD filament formation, which in turn serves as a signaling platform to recruit and activate downstream signaling molecules, such as TBK1 and IRF3 (*16, 17*).

The notion that RIG-I signaling requires both the release of 2CARD auto-repression and the tetramerization of 2CARD is further supported by the presence of multiple mechanisms that modulate RIG-I oligomerization (*11, 15*). In particular, K63-linked polyubiquitin (K63-$Ub_n$) was

shown to play an important role in efficient RIG-I signaling by stabilizing the RIG-I 2CARD tetramer (*15*). Structural studies further showed that K63-$Ub_n$ chains bind the periphery of the core 2CARD tetramer, bridging the adjacent subunits and stabilizing the 2CARD tetramer (*14*). The tetramer then acts as a helical template to nucleate the MAVS filament formation (*17*). Despite the detailed understanding of the action of Ub on RIG-I, much remains debated about how and when Ub is placed on RIG-I, and which E3 ligase is involved. Previous studies, including knock-out mice studies, reported TRIM25 and RIPLET (*i.e.* RNF135) as two essential E3 ligases in RIG-I signaling (*18-21*), but their relationships and interactions with RIG-I remained unclear.

To examine the importance of RIPLET and TRIM25 in RIG-I functions, we first measured the signaling activity of RIG-I in wild-type (WT) 293T cells and those lacking RIPLET or TRIM25. Knocking out RIPLET, but not TRIM25, abrogated RIG-I signaling in response to various RIG-I stimulants, such as *in vitro* transcribed dsRNAs with 5'ppp and Sendai virus (SeV), as measured by the IFNβ promoter reporter activity or the IFNβ mRNA level (Fig. 1, A and B, fig. S1A). Ectopic expression of RIPLET restored RIG-I signaling in $RIPLET^{-/-}$ cells, while TRIM25 had little impact on RIG-I signaling in $TRIM25^{-/-}$ cells (fig. S1A). Neither $RIPLET^{-/-}$ nor $TRIM25^{-/-}$ cells displayed any defect in MDA5- or MAVS-mediate antiviral signaling (fig. S1B). The RNA-independent signaling activity of RIG-I 2CARD fused to GST (GST-2CARD) was also unaffected by RIPLET or TRIM25 knock-out (fig. S1C), although ectopic expression of TRIM25 does stimulate GST-2CARD signaling (fig. S1D) (*18*). Thus, full-length RIG-I signaling requires RIPLET, not TRIM25, while GST-2CARD activates antiviral signaling through a different, RIPLET-independent manner.

To test whether RIPLET or TRIM25 can directly conjugate K63-$Ub_n$ to RIG-I, we reconstituted the RIG-I ubiquitination reaction *in vitro*. Previous studies showed that RIG-I signaling requires Ubc13 (*i.e.* Ube2N) (*22*), an Ub E2 conjugating enzyme that can function either by itself or in complex with catalytically inactive E2 variants, such as Uev1A (*i.e.* Ube2V1) (*23*). Incubation of RIG-I with purified E1, E2(s), and RIPLET (or TRIM25) shows that Ubc13:Uev1A, but not Ubc13 alone, supported robust polyubiquitination of RIG-I (Fig. 1C). The K63R mutation in Ub prevented polyUb chain conjugation, suggesting that RIPLET conjugates K63-$Ub_n$ to RIG-I (fig. S2A). Intriguingly, ubiquitination of RIG-I was greatly stimulated by dsRNA (Fig. 1C). Since RIPLET does not bind dsRNA (fig. S2B), this result implies that RIPLET recognizes dsRNA-bound RIG-I. Consistent with the lack of impact of TRIM25 on RIG-I signaling (Fig. 1, A and B), no RIG-I ubiquitination was observed with TRIM25 under the equivalent condition (Fig. 1C), despite the robust auto-ubiquitination of TRIM25 (fig. S2C). To examine whether RIPLET-mediated Ub-conjugation can activate RIG-I, we employed the MAVS polymerization assay (*11, 24*). In this assay, purified RIG-I was mixed with isolated, monomeric MAVS CARD and the RIG-I signaling activity was measured by the monomer-to-filament transition of MAVS using native gel electrophoresis and electron microscopy (EM). The result shows that RIG-I stimulates MAVS polymerization in a manner that depends on both dsRNA and RIPLET (Fig. 1, D and E).

Previous studies showed that RIPLET in conjunction with the Ubc13:Uev1A complex synthesizes unanchored Ub chains (*22*). We found that RIPLET indeed promotes unanchored $Ub_n$ synthesis, but that this activity is independent of RIG-I and is suppressed by the RIG-I:RNA

complex (fig. S2D). This suggests that unanchored $Ub_n$ synthesis occurs constitutively, while this mode of $Ub_n$ synthesis shifts to RIG-I-anchored $Ub_n$ synthesis upon its binding to the RIG-I:dsRNA complex. In addition, anchored $Ub_n$ alone appears to be sufficient for RIG-I signaling; RIG-I maintained a significant level of the MAVS polymerzation activity even after treatment with isoT (fig. S2, E and F), an ubiquitin-processing protease with a known preference for unanchored $Ub_n$. We note that isoT also partially degraded anchored $Ub_n$ (fig. S2E), which could partly explain the reduction of MAVS polymerzation upon isoT treatment. Consistent with the notion that RIPLET-mediated Ub conjugation can activate RIG-I, mass spectrometric analysis showed that RIPLET ubiquitinates RIG-I at K190 and K193 in 2CARD, which are located in close proximity to the Ub binding site on 2CARD (fig. S2G). Altogether, our data show that RIPLET is an essential E3 ligase that ubiquitinates RIG-I in a dsRNA-dependent manner. Moreover, RIPLET-mediated ubiquitination activates RIG-I, although the potential contribution of unanchored $Ub_n$ cannot be excluded.

We next explored how RIPLET interacts with RIG-I and how this interaction depends on dsRNA. We purified recombinant RIPLET and RIG-I (fig. S3A), and used native gel shift assays to examine the mobility of fluorescently labeled RIG-I with and without RIPLET. Consistent with the dsRNA-dependent ubiquitination of RIG-I (Fig. 1C), RIPLET bound RIG-I only in the presence of dsRNAs (Fig. 2A). Furthermore, the N-terminal 2CARD truncation mutant (RIG-IΔN) also bound RIPLET in a manner dependent on dsRNA. Isolated 2CARD did not bind RIPLET (Fig. 2A), in agreement with the lack of effect of RIPLET on GST-2CARD signaling (fig. S1C). Further truncation of RIG-I to the helicase domain or CTD impaired RIPLET binding (fig. S3B), indicating that RIG-IΔN is minimally required. For a more detailed analysis, we

compared RIPLET binding to RIG-I in complex with 15, 21, 42, 62, and 162 bp dsRNAs, which can accommodate 1, 2, 3, 4-5 and 11-12 RIG-I molecules, respectively (Fig. 2B). The mobility shift assay showed that RIPLET binding requires at least 21 bp dsRNA, *i.e.* two RIG-IΔN molecules in proximity.

RIPLET consists of the N-terminal RING, central coiled coil (CC) and C-terminal Pry/Spry (PSpry) domains (Fig. 2B). The RING domain is known to recognize E2 conjugating enzymes, and is essential for both RIG-I ubiquitination and unanchored $Ub_n$ synthesis (fig. S3C). RING deletion (ΔRING) had little impact on RIG-I binding (Fig. 2B), consistent with the role of RING in E2 engagement rather than substrate binding. Further deletion of the CC domain, however, abolished RIG-I binding (Fig. 2C). Since CC is responsible for dimerization of RIPLET (fig. S3D), we examined the importance of the dimeric state by replacing CC by GST. The GST-PSpry fusion fully restored RIG-I binding (Fig. 2C and fig. S3E), suggesting that PSpry is the RIG-I binding domain, and bivalency is required for high affinity binding (Fig. 2D). This is in line with the observation that RIPLET binds RIG-I only in complex with dsRNA long enough to accommodate at least two RIG-I molecules (Fig. 2B).

This bivalent binding mode of RIPLET predicts that RIPLET binds RIG-I filaments on longer dsRNA more stably, as longer filaments would allow many more RIPLET binding configurations (Fig. 2D). At the same time, RIG-I filament assembly on >~1 kb dsRNAs is known to be inefficient (due to its assembly from the dsRNA end) (*11*), implying that RIPLET binding on very long (>~1 kb) dsRNA would be similarly limited. In overall agreement with both of these predictions, RIG-I ubiquitination and signaling displayed a bell-shaped length-

dependence, when compared at equivalent RNA mass concentrations (Fig. 2, E and F). RIG-I ubiquitination, however, showed the peak efficiency around 30-40 bp, which is unexpectedly short given the efficient RIG-I filament formation on longer dsRNA under ~500 bp (*11*). The dsRNA length for maximal ubiquitination was also less than the dsRNA length at which maximal RIG-I signaling was observed (60-160 bp) (Fig. 2F). These apparent mismatches raised the question of whether RIPLET binds RIG-I filaments on >~40 bp dsRNA differently, perhaps in a manner non-conducive for ubiquitination, but still conducive for RIG-I signaling. Intriguingly, with 512 bp dsRNAs, we often observed two populations of RIG-I:RIPLET complexes in native gels: those migrating into the gel and those remaining in the gel well (fig. S3F).

To examine how RIPLET binds RIG-I filaments on long dsRNAs and whether RIPLET can induce additional higher-order oligomerization of RIG-I, we employed negative stain EM to visually inspect RIPLET:RIG-I complexes formed on 512 bp dsRNA. The results showed that RIPLET can cross-bridge RIG-I filaments and promote aggregation of RIG-I filaments (Fig. 3A). Non-crosslinked, individual RIG-I filaments were also visible, which are likely a combination of RIPLET-free RIG-I filaments and those bound by RIPLET in the intra-filament manner (as illustrated in Fig. 2D). As with the intra-filament binding mode, inter-filament cross-linking was induced by ΔRING as efficiently as full-length RIPLET (Fig. 3A). 2CARD in RIG-I was also dispensable for RIG-I filament bridging by RIPLET (fig. S4A). No such aggregate structure was observed in the absence of dsRNA (fig. S4A) or with MDA5 filaments (fig. S4B).

Intriguingly, GST-PSpry, which binds RIG-I as efficiently as ΔRING (fig. S3E), did not promote RIG-I filament bridging (Fig. 3B). The ability of ΔRING, but not GST-PSpry, to induce RIG-I filament bridging was also confirmed by an independent pull-down analysis. Here, RIG-IΔN and ΔRING (or GST-PSpry) were incubated with a mixture of 3'-biotinylated 112 bp dsRNA and non-biotinylated 162 bp dsRNA, and the 112 bp dsRNA-bound complex was purified with streptavidin beads (Fig. 3C). Eluate analysis showed that non-biotinylated 162 bp dsRNA co-purifies with biotinylated 112 bp dsRNA only when ΔRING and RIG-IΔN are jointly present, further supporting the notion that ΔRING bridges RIG-I filaments (Fig. 3C). GST-PSpry did not promote association between 112 bp and 162 bp dsRNAs, consistent with the EM result (Fig. 3B) showing that GST-PSpry does not cross-bridge RIG-I filaments.

To understand how RIPLET CC, but not GST, allows for RIG-I filament bridging, we further examined other types of dimeric CCs. The PSpry domain fused with an artificial CC adopted from *Arabidopsis thaliana* Mom1 (MCC-PSpry, fig. S4C) also induced RIG-I filament bridging, as indicated by co-purification of 112 bp and 162 bp dsRNAs (fig. S4D). PSpry fused with the CC domain from *Saccharomyces cerevisiae* Gal4 (GCC-PSpry), by contrast, did not bridge RIG-I filaments (fig. S4D). Note that the RIPLET CC is a ~64 amino acid (aa)-long dimer that is most likely in the antiparallel orientation (fig. S4, E and F), and MCC is a 141 aa-long antiparallel dimer (*25*). By contrast, GST is a globular dimer and GCC is a short (16 aa) parallel CC (*26*) (fig. S4C). Based on these observations, we speculate that the abilities of RIPLET CC and MCC to cross-bridge RIG-I filaments stem from weak interactions between long antiparallel CCs, which may stabilize transient multivalent RIPLET oligomers when locally concentrated on a RIG-I filament (Fig. 3D).

We next asked whether RIPLET-mediated bridging of RIG-I filaments also occurs in cells. Previous studies showed that RIG-I forms aggregate-like granules upon infection with various viruses (*27, 28*) and this granule formation correlates with IRF3 nuclear localization (*27*), but the underlying mechanism was unknown. We found similar granule formation with endogenous RIG-I in 293T, HeLa, and bone-marrow-derived mouse macrophages (BMDMs) upon 5'ppp-dsRNA transfection or SeV infection (Fig. 3E & fig. S5A). Depending on the cell types and stimuli, some RIG-I granules co-localized with TIAR-stained stress granules (SGs), while others did not (fig. S5, B to D). Even in the case where RIG-I granules co-localize with SGs, RIG-I granule formation preceded SG formation (fig. S5C) (*27*), suggesting that SG formation is unlikely to be the driving factor for RIG-I granule formation. Intriguingly, RIG-I granule formation was greatly impaired by RIPLET knock-out in 293T (Fig. 3E). Ectopic expression of HA-tagged RIPLET in RIPLET$^{-/-}$ 293T cells restored RIG-I granule formation, which co-localized with RIPLET (Fig. 3F). ΔRING also restored RIG-I granule formation, suggesting that RIPLET-mediated filament bridging underlies the RIG-I granule assembly.

Next, we investigated whether filament bridging contributes to RIG-I signaling. We hypothesized that such clustering of RIG-I molecules would promote 2CARD tetramerization and thus, MAVS activation, either with or without K63-Ub$_n$. To first test the Ub-independent role of filament bridging, we asked whether ΔRING, which can bridge RIG-I filaments but cannot ubiquitinate RIG-I (fig. S3C, and fig. S4A), enhances RIG-I signaling. Ectopic expression of RIPLET in RIPLET$^{-/-}$ cells restored RIG-I signaling upon stimulation with dsRNA or SeV infection (Fig. 4, A and B). Intriguingly, ΔRING also partially restored RIG-I signaling, albeit

not as effectively as full-length RIPLET does (Fig. 4, A and B). ΔRING-mediated amplification of RIG-I signaling is more pronounced with longer RNA (Fig. 4C), as expected for the filament bridging-mediated activity.

To examine whether the positive effect of ΔRING is indeed mediated by inter-filament bridging vs. intra-filament binding, we used CC-swap mutants of ΔRING, which showed different levels of filament bridging (Fig. 3, A to C, and fig. S4D). As with ΔRING, MCC-PSpry robustly stimulated RIG-I signaling, but GST-PSpry and GCC-PSpry had a moderate effect on RIG-I (Fig. 4D). The effects of these RIPLET variants on RIG-I signaling paralleled their abilities to bridge RIG-I filaments. To further test the impact of RIG-I filament cross-bridging in antiviral signaling, we used PSpry fused to four tandem repeats of FKBP (4xFKBP), which is known to aggregate upon binding to a chemical dimerizer (*i.e.* AP1903) (fig. S6A) (*29, 30*). Consistent with the importance of RIG-I aggregation, RIG-I signaling in response to SeV was stimulated by 4xFKBP-PSpry only in the presence of AP1903 (fig. S6A). PSpry without the 4xFKBP fusion did not stimulate RIG-I with or without AP1903. Altogether, the results show that RIPLET can amplify RIG-I signaling by cross-bridging RIG-I filaments independent of Ub.

To more directly test the importance of RIG-I filament bridging in antiviral signaling, we employed the *in vitro* MAVS polymerization assay as in Fig, 1, D and E. Because this assay utilizes only the purified proteins and RNA, it allowed a direct test of the impact of ΔRING on RIG-I signaling in the absence of other cellular components. Since K63-$Ub_n$ can be introduced *in trans*, this assay also allowed us to measure the effect of RIG-I filament bridging, both with and without K63-$Ub_n$. Consistent with the notion that RIG-I filament bridging can stimulate RIG-I

signaling, MAVS filament formation was stimulated by ΔRING, but not by GST-PSpry, in the absence of K63-$Ub_n$ (Fig. 4E). Similar stimulatory activity of ΔRING was observed even with a broad range of K63-$Ub_n$ (Fig. 4F), suggesting that filament bridging is an important aspect of the RIPLET function, regardless of its ubiquitination activity. Consistent with this notion, full-length RIPLET, which can both ubiquitinate RIG-I and bridge RIG-I filaments, is a more potent stimulator of RIG-I than is RING fused to GST-PSpry (fig. S6B), which can bind but not bridge RIG-I filaments (Fig. 3, B and C). Altogether, our findings demonstrate that RIPLET contributes to RIG-I signaling through at least two synergistic mechanisms: RIG-I ubiquitination and RIG-I filament cross-bridging (Fig. 4G). The combination of these effects likely underlies the bell-shaped dsRNA length dependence.

In the conventional view of RIG-I activation, ubiquitination of RIG-I linearly follows ligand selection by RIG-I. That is, dsRNA binding releases RIG-I 2CARD, which then allows an E3 ligase to bind and ubiquitinate exposed 2CARD for signal activation. We here show that RIPLET functions as a co-receptor, rather than a downstream accessory protein, that actively participates in both RNA-discrimination and receptor oligomerization. It does so by preferentially binding to filamentous oligomers of RIG-I on >20 bp dsRNA and by cross-bridging RIG-I filaments in both Ub-dependent and -independent manners to induce higher-order receptor "clustering". This clustering mechanism of RIG-I provides a new perspective on receptor clustering, a phenomenon studied primarily in the context of cell-surface receptors (*31*). Our discovery of the Ub-independent function of RIPLET, which synergizes with the canonical Ub-conjugation activity for efficient RIG-I signaling, also challenges the conventional view that E3 ligases function primarily through Ub chain synthesis.

Our work also addresses the long-debated question on the identity of the E3 ligase essential for RIG-I function. By using a combination of functional assays and biochemistry, we have unambiguously identified the critical role of RIPLET, not TRIM25, in RIG-I signaling in response to dsRNAs and SeV. This is also in line with the previous report that IFNβ induction in response to Vesicular stomatitis virus is impaired in RIPLET$^{-/-}$ cells, but not in TRIM25$^{-/-}$ cells [22]. Considering the growing list of RIG-I-independent antiviral functions of TRIM25 – mediated by its RNA binding activity (*32-34*) and its interaction partner ZAP (*35, 36*)– the precise nature of the observed effect of TRIM25 on RIG-I requires more detailed investigation.

Finally, our findings offer new perspectives on membrane-less granules found in an increasingly broad range of biological processes. These include stress granules and nuclear speckles, which utilize multivalent interactions inherent in intrinsic disordered regions (IDRs) or domain repeats (*37*). Our findings show that RIG-I granules form even without such IDRs or domain repeats, but in a hierarchical manner where multivalent interactions emerge only upon ligand binding. That is, dsRNA acts as an initial scaffold for RIG-I filament assembly, which then functions as a secondary scaffold to recruit bivalent RIPLET for RIG-I filament bridging and RIG-I granule assembly. Since each step can serve as a check-point for ligand discrimination, this multi-step assembly would enable highly regulated aggregation and signal amplification. Additionally, our discovery of a dimeric E3 ligase acting as a "molecular glue" in membrane-less granule assembly raises an intriguing possibility of a broad range of dimeric CC E3 ligases (*e.g.* TRIM proteins) functioning in analogous manners (*38*). Together, our findings

highlight previously unrecognized non-canonical functions of E3 ligases in protein aggregation and innate immune ligand discrimination.

**Acknowledgement**

We thank Dr. M.Gack for sharing TRIM25$^{-/-}$ 293T cells, and Dr. O.Pornillos for sharing the TRIM25 construct and protein purification protocol. This work was supported by NSF fellowship (C.C.), Cancer Research Institute fellowship (S.A.), German Academic Exchange Service PROMOS program (A.X.), Japan Society for the Promotion of Science Core to core program (T.F.), Burroughs Wellcome Fund and NIH grants (R01AI106912, R01AI111784 and R21AI130791) (S.H.).

**Author contributions**

CC, SA, AX and SH designed experiments and analyzed data. CC, SA, AX, JWP performed experiments. FH provided RIPLET$^{-/-}$ 293T, and FH, TF, SO provided antibodies for RIPLET, RIG-I and IRF3.

**References**

1. M. Yoneyama, T. Fujita, Recognition of viral nucleic acids in innate immunity. *Rev. Med. Virol.* **20**, 4-22 (2010).
2. D. Goubau, S. Deddouche, C. Reis e Sousa, Cytosolic Sensing of Viruses. *Immunity* **38**, 855-869 (2013).
3. D. Goubau *et al.*, Antiviral immunity via RIG-I-mediated recognition of RNA bearing 5'-diphosphates. *Nature* **514**, 372-375 (2014).

4. M. Schlee *et al.*, Recognition of 5'triphosphate by RIG-I helicase requires short blunt double-stranded RNA as contained in panhandle of negative-strand virus. *Immunity* **31**, 25-34 (2009).

5. D. C. Rawling, A. M. Pyle, Parts, assembly and operation of the RIG-I family of motors. *Curr Opin Struct Biol* **25**, 25-33 (2014).

6. J. Sohn, S. Hur, Filament assemblies in foreign nucleic acid sensors. *Curr Opin Struct Biol* **37**, 134-144 (2016).

7. C. Lassig, K. P. Hopfner, Discrimination of cytosolic self and non-self RNA by RIG-I-like receptors. *J Biol Chem* **292**, 9000-9009 (2017).

8. E. Kowalinski *et al.*, Structural basis for the activation of innate immune pattern-recognition receptor RIG-I by viral RNA. *Cell* **147**, 423-435 (2011).

9. D. Luo, A. Kohlway, A. Vela, A. M. Pyle, Visualizing the determinants of viral RNA recognition by innate immune sensor RIG-I. *Structure* **20**, 1983-1988 (2012).

10. F. Jiang *et al.*, Structural basis of RNA recognition and activation by innate immune receptor RIG-I. *Nature* **479**, 423-427 (2011).

11. A. Peisley, B. Wu, H. Yao, T. Walz, S. Hur, RIG-I Forms Signaling-Competent Filaments in an ATP-Dependent, Ubiquitin-Independent Manner. *Mol Cell* **51**, 573-583 (2013).

12. J. R. Patel *et al.*, ATPase-driven oligomerization of RIG-I on RNA allows optimal activation of type-I interferon. *EMBO Rep.* **14**, 780-787 (2013).

13. D. C. Rawling, M. E. Fitzgerald, A. M. Pyle, Establishing the role of ATP for the function of the RIG-I innate immune sensor. *Elife* **4**, (2015).

14. A. Peisley, B. Wu, H. Xu, Z. J. Chen, S. Hur, Structural basis for ubiquitin-mediated antiviral signal activation by RIG-I. *Nature* **509**, 110-114 (2014).

15. X. Jiang *et al.*, Ubiquitin-Induced Oligomerization of the RNA Sensors RIG-I and MDA5 Activates Antiviral Innate Immune Response. *Immunity* **36**, 959-973 (2012).

16. F. Hou *et al.*, MAVS forms functional prion-like aggregates to activate and propagate antiviral innate immune response. *Cell* **146**, 1-14 (2011).

17. B. Wu *et al.*, Molecular imprinting as a signal activation mechanism of the viral RNA sensor RIG-I. *Mol Cell* **55**, 511-523 (2014).

18. M. U. Gack *et al.*, TRIM25 RING-finger E3 ubiquitin ligase is essential for RIG-I-mediated antiviral activity. *Nature* **446**, 916-920 (2007).

19. D. Gao *et al.*, REUL is a novel E3 ubiquitin ligase and stimulator of retinoic-acid-inducible gene-I. *PLoS One* **4**, e5760 (2009).

20. H. Oshiumi, M. Matsumoto, S. Hatakeyama, T. Seya, Riplet/RNF135, a RING finger protein, ubiquitinates RIG-I to promote interferon-beta induction during the early phase of viral infection. *J Biol Chem* **284**, 807-817 (2009).

21. H. Oshiumi *et al.*, The ubiquitin ligase Riplet is essential for RIG-I-dependent innate immune responses to RNA virus infection. *Cell Host Microbe* **8**, 496-509 (2010).

22. Y. Shi *et al.*, Ube2D3 and Ube2N are essential for RIG-I-mediated MAVS aggregation in antiviral innate immunity. *Nat Commun* **8**, 15138 (2017).

23. X. Wu, M. Karin, Emerging roles of Lys63-linked polyubiquitylation in immune responses. *Immunol Rev* **266**, 161-174 (2015).

24. B. Wu *et al.*, Structural Basis for dsRNA Recognition, Filament Formation, and Antiviral Signal Activation by MDA5. *Cell* **152**, 276-289 (2013).

25. T. Nishimura *et al.*, Structural basis of transcriptional gene silencing mediated by Arabidopsis MOM1. *PLoS Genet* **8**, e1002484 (2012).

26. R. Marmorstein, M. Carey, M. Ptashne, S. C. Harrison, DNA recognition by GAL4: structure of a protein-DNA complex. *Nature* **356**, 408-414 (1992).

27. S. W. Oh *et al.*, Leader-Containing Uncapped Viral Transcript Activates RIG-I in Antiviral Stress Granules. *PLoS Pathog* **12**, e1005444 (2016).

28. M. T. Sanchez-Aparicio, J. Ayllon, A. Leo-Macias, T. Wolff, A. Garcia-Sastre, Subcellular Localizations of RIG-I, TRIM25, and MAVS Complexes. *J Virol* **91**, (2017).

29. T. Clackson *et al.*, Redesigning an FKBP-ligand interface to generate chemical dimerizers with novel specificity. *Proc Natl Acad Sci U S A* **95**, 10437-10442 (1998).

30. D. M. Spencer, T. J. Wandless, S. L. Schreiber, G. R. Crabtree, Controlling signal transduction with synthetic ligands. *Science* **262**, 1019-1024 (1993).

31. N. C. Hartman, J. T. Groves, Signaling clusters in the cell membranes. *Curr Opin Cell Biol* **23**, 370-376 (2011).

32. N. R. Choudhury *et al.*, Trim25 Is an RNA-Specific Activator of Lin28a/TuT4-Mediated Uridylation. *Cell Rep* **9**, 1265-1272 (2014).

33. G. Manokaran *et al.*, Dengue subgenomic RNA binds TRIM25 to inhibit interferon expression for epidemiological fitness. *Science* **350**, 217-221 (2015).

34. N. R. Meyerson *et al.*, Nuclear TRIM25 Specifically Targets Influenza Virus Ribonucleoproteins to Block the Onset of RNA Chain Elongation. *Cell Host Microbe* **22**, 627-638 e627 (2017).

35. M. M. Li *et al.*, TRIM25 Enhances the Antiviral Action of Zinc-Finger Antiviral Protein (ZAP). *PLoS Pathog* **13**, e1006145 (2017).

36. X. Zheng *et al.*, TRIM25 Is Required for the Antiviral Activity of Zinc Finger Antiviral Protein. *J Virol* **91**, (2017).

37. S. F. Banani, H. O. Lee, A. A. Hyman, M. K. Rosen, Biomolecular condensates: organizers of cellular biochemistry. *Nat Rev Mol Cell Biol* **18**, 285-298 (2017).

38. R. Rajsbaum, A. Garcia-Sastre, G. A. Versteeg, TRIMmunity: the roles of the TRIM E3-ubiquitin ligase family in innate antiviral immunity. *J Mol Biol* **426**, 1265-1284 (2014).

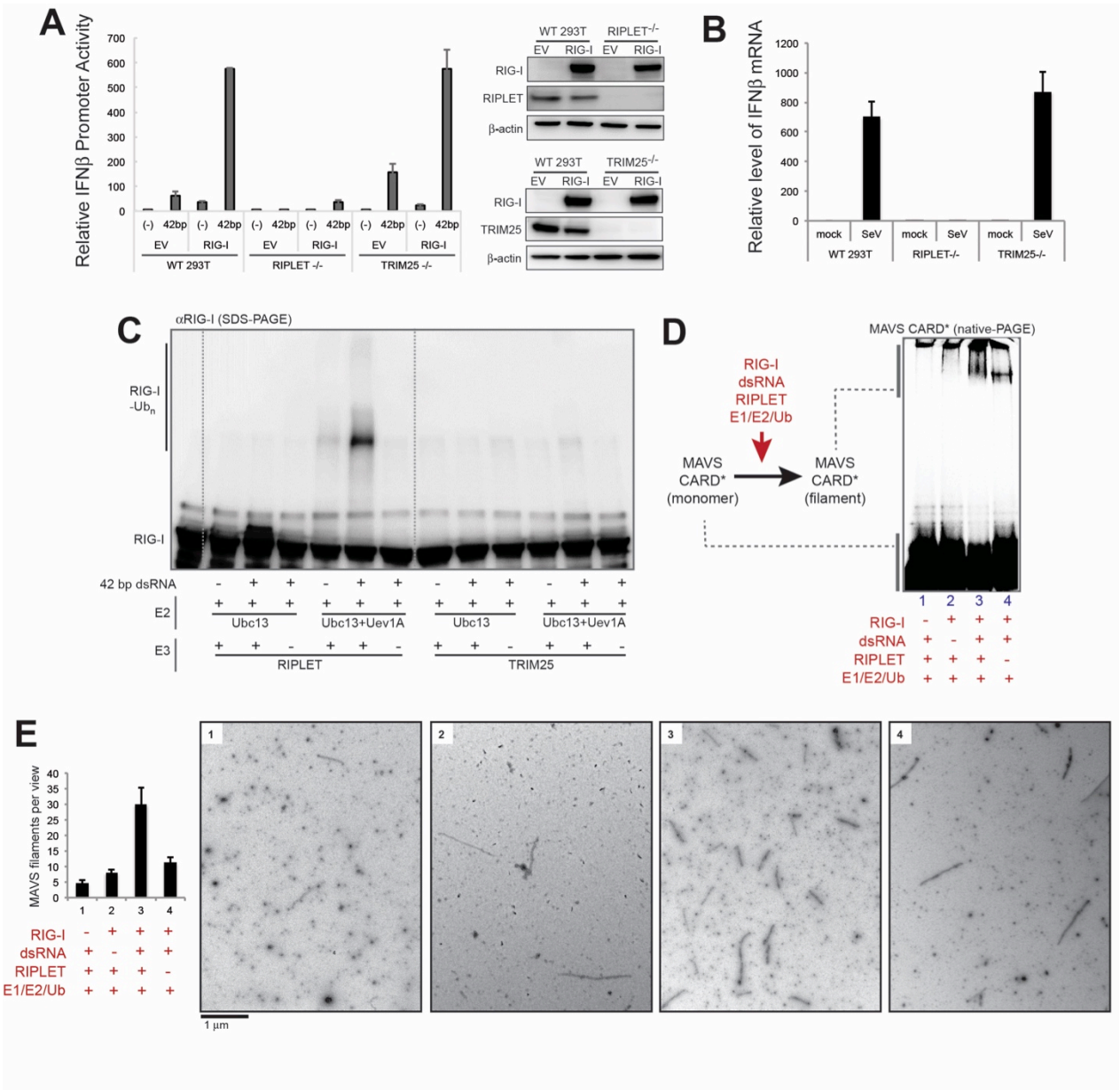


**Fig. 1 RIPLET, not TRIM25, ubiquitinates RIG-I for antiviral signal activation.**

A. Relative RIG-I signaling activity as measured by the IFNβ promoter reporter assay (mean ± s.d., $n = 3$). 293T cells (WT, RIPLET$^{-/-}$ or TRIM25$^{-/-}$) were transfected with empty vector (EV) or the RIG-I expression plasmid (10 ng), and stimulated with 42 bp dsRNA with 5'ppp (0.2 μg) prior to the reporter activity measurement. All RNAs in this study harbor 5'ppp, unless mentioned otherwise. Right: western blot (WB) showing deletion of respective genes.

B. Relative level of endogenous RIG-I signaling upon SeV infection (100 HA units/ml), as measured by the IFNβ mRNA level (mean ± s.d., $n = 3$).

C. *In vitro* ubiquitination analysis of RIG-I. Purified E1, E2 (Ubc13 alone or in complex with Uev1A, 5 and 2.5 μM, respectably), E3 (RIPLET or TRIM25, 0.25 μM) and Ub (20 μM) were incubated with RIG-I (0.5 μM), either alone or in complex with 42 bp dsRNA (1 ng/μl). Ubiquitination of RIG-I was analyzed by anti-RIG-I blot on SDS gels.

D-E. RIG-I-induced MAVS polymerization assay. The RIG-I ubiquitination reaction was performed as in (C), and was mixed with purified, monomeric MAVS CARD fused to the fluorescent SNAP tag (10 μM). Monomer-to-filament transition of MAVS CARD was analyzed by native gel assay (D) or negative stain EM (E). For EM analysis, six random images (representative images shown on the right) were collected at 4,800x magnification, and average number (± s.d) of filaments per image was plotted on the left.

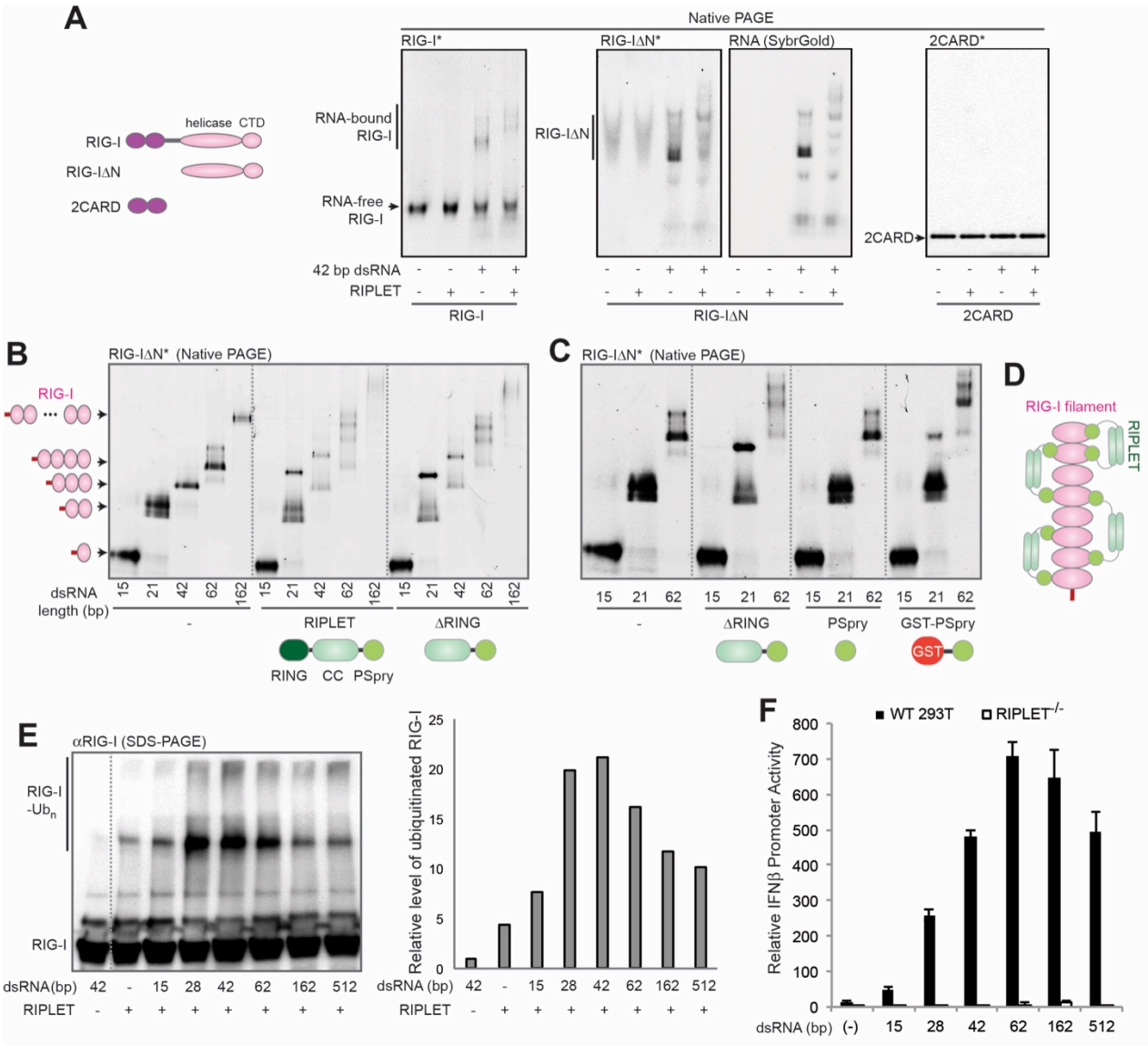


**Fig. 2 RIPLET recognizes pre-oligomerized RIG-I on dsRNA and activates RIG-I signaling in a dsRNA length-dependent manner.**

A. Native gel shift assay to monitor the RIG-I:RIPLET interaction. Fluorescently labeled RIG-I (full-length RIG-I, RIG-IΔN or isolated 2CARD, 0.5 μM) was incubated with RIPLET (0.5 μM) in the presence or absence of 42 bp dsRNA (1 ng/μl), and the complex was analyzed by native gel using RIG-I fluorescence (*). For RIG-IΔN, SybrGold stained image was also shown to clearly visualize only the RNA-bound species.

B-C. Native gel shift assay of RIG-IΔN (0.5 μM) with and without RIPLET (b), ΔRING (b, c), PSpry (c) or GST-PSpry (c) (0.5 μM for all RIPLET variants). 15-162 bp dsRNAs (1 ng/μl) were used to form RIG-I:RNA complexes of different size.

D. A model of how RIPLET binds RIG-I filaments. Based on the dsRNA length dependence and bivalency requirement, we propose that RIPLET binds two nearby RIG-I monomers within a filament (either immediately adjacent or separated). The lengths of RIPLET CC

(~60 amino acids, expected to be ~80 Å) and the linker between CC and PSpry (~50 amino acids, expected to be >100 Å for fully disordered linker) are compatible with the model.

E. *In vitro* ubiquitination analysis of RIG-I in the presence of 15-512 bp dsRNAs (1 ng/μl for all RNAs), as performed in Fig. 1c. Right: densitometry analysis of ubiquitinated RIG-I.

F. Relative RIG-I signaling activity in response to 15-512 bp dsRNA (0.2 μg for all RNAs) in 293T cells (WT or RIPLET$^{-/-}$) using transiently expressed RIG-I, as measured by the IFNβ promoter reporter assay (mean ± s.d., $n$ = 3).

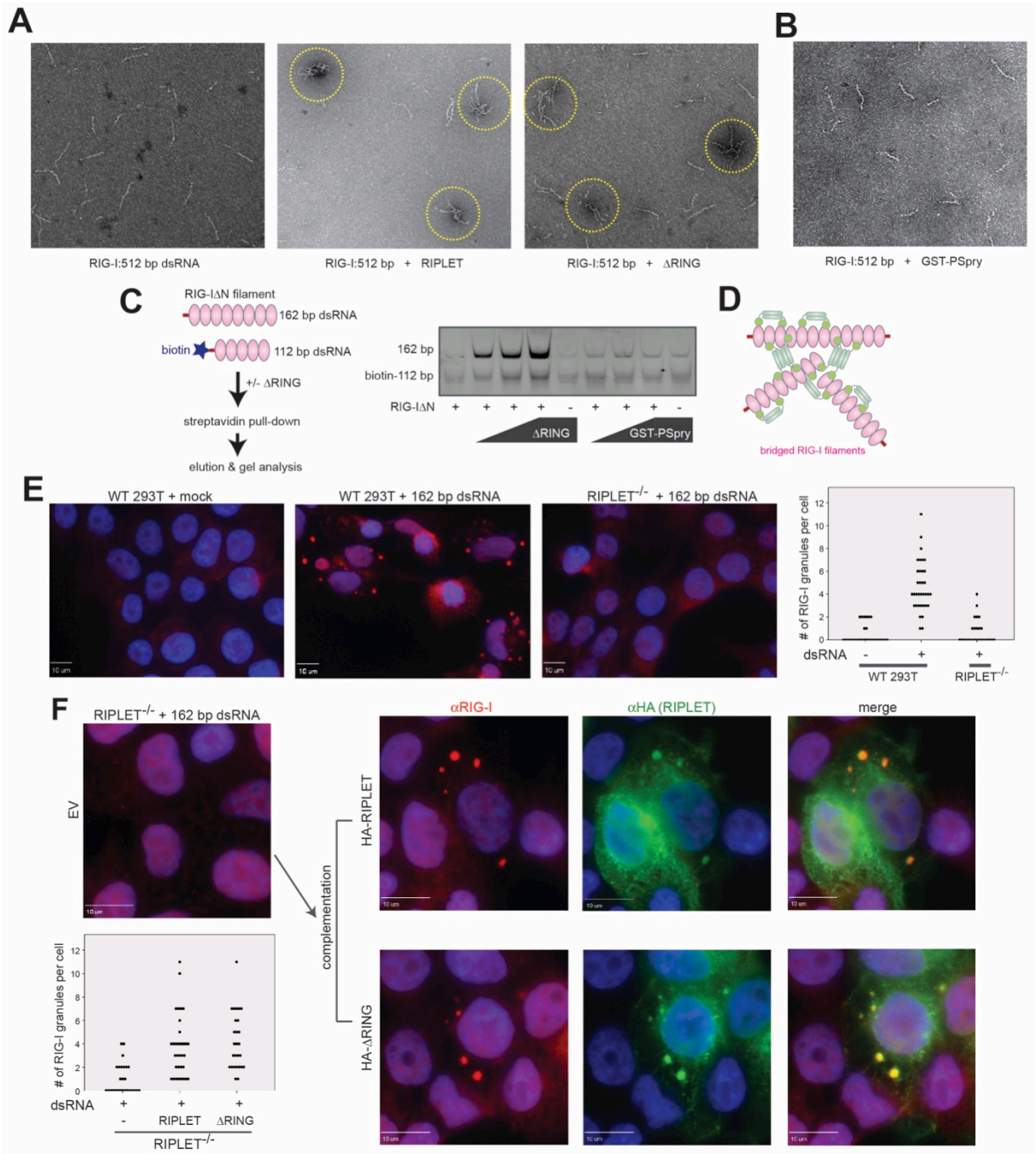


**Fig. 3 RIPLET cross-bridges RIG-I filaments on long dsRNAs, and promotes RIG-I granule assembly *in vivo***

A. Representative EM images of RIG-I filaments (0.5 μM) formed on 512 bp dsRNA (1 ng/μl), in the presence and absence of RIPLET or ΔRING (0.5 μM). Cross-bridged RIG-I filaments are highlighted with yellow circles.

B. Representative EM image of RIG-I filaments (0.5 μM) formed on 512 bp dsRNA (1 ng/μl), in the presence of GST-PSpry (0.5 μM).

C. Streptavidin pull-down analysis to examine RIPLET-mediated cross-bridging of RIG-I filaments. RIG-IΔN filaments (0.5 μM) were formed on non-biotinylated 162 bp dsRNA (1 ng/μl) and 3'-biotinylated 112 bp dsRNA (1 ng/μl), and were incubated with an increasing concentration of ΔRING or GST-PSpry (0.25, 0.5, and 1 μM). Biotinylated 112 bp dsRNA was purified using streptavidin beads and co-purified 162 bp dsRNA was analyzed on the gel.
D. A model of RIG-I filament cross-bridging by RIPLET. Weak inter-molecular interactions between coiled coils (CCs) may allow RIPLET to cross-bridge distinct RIG-I filaments. Note that the two binding modes, intra-filament binding (in Fig. 2d) and inter-filament bridging (Fig. 3d), are not mutually exclusive and can co-occur on the same RIG-I filament.
E. Immunofluorescence analysis of endogenous RIG-I granules in 293T cells (wild-type or RIPLET$^{-/-}$) 2 hrs after stimulation with 5'ppp-162 bp dsRNA. Right: quantitation of number of RIG-I granules per cell with and without dsRNA in 293T or RIPLET$^{-/-}$.
F. RIPLET complementation analysis. RIG-I granule assembly was examined in RIPLET$^{-/-}$ 293T cells after transfection with empty vector (EV) or plasmids expressing HA-tagged full-length RIPLET or ΔRING. Left bottom: quantitation of number of RIG-I granules per cell before and after complementation. All cells were stimulated with 5'ppp-162 bp dsRNA.

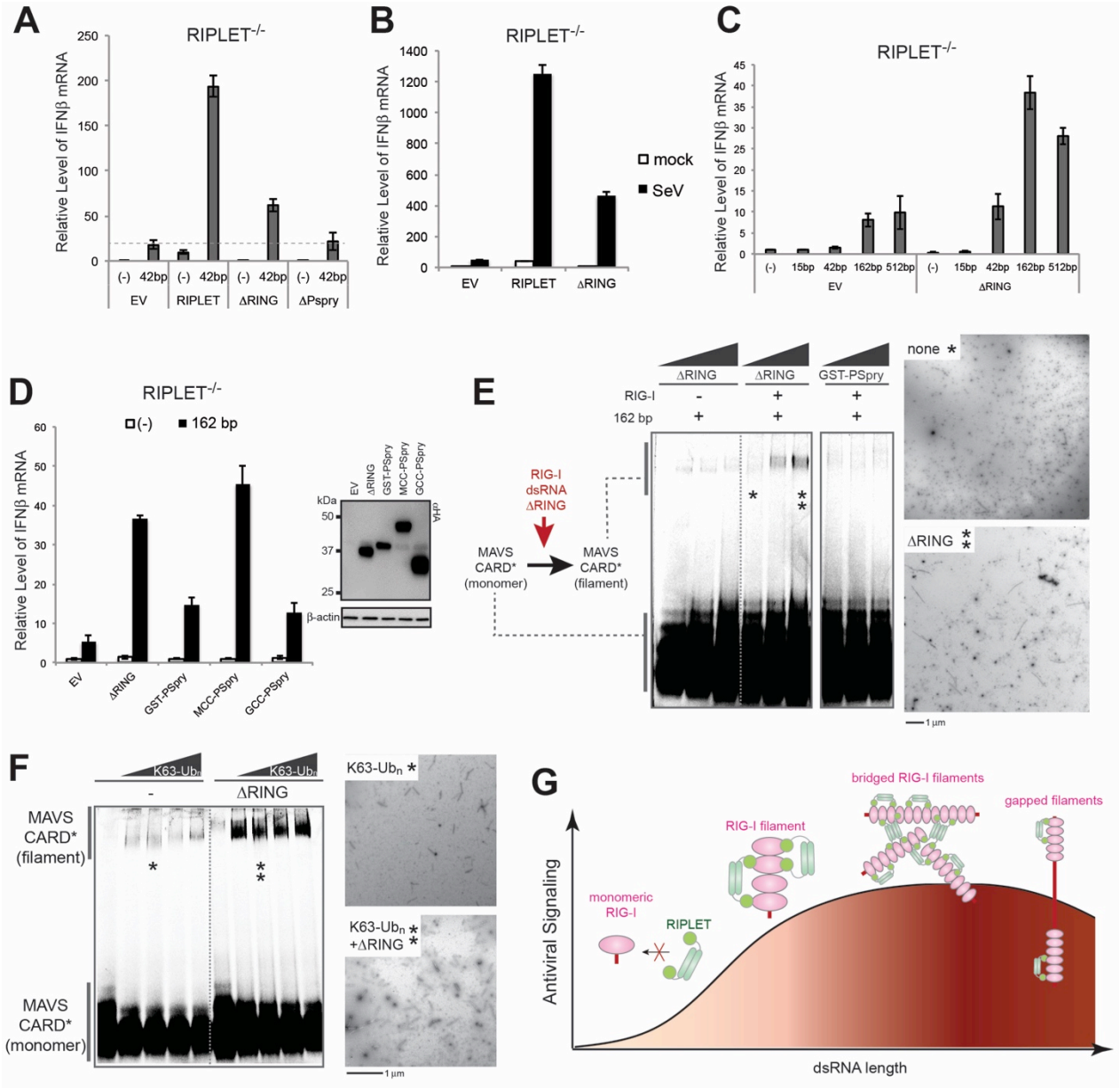


**Fig. 4 RIPLET-mediated RIG-I aggregation enhances antiviral signaling, in both ubiquitin-dependent and -independent manners.**

A. Relative level of RIG-I signaling upon stimulation with 42 bp dsRNA (0.2 μg) in RIPLET$^{-/-}$ 293T cells complemented with empty vector (EV), RIPLET, ΔRING or ΔPSpry (20 ng). The level of antiviral signaling was measured by IFNβ mRNA (mean ± s.d., $n$ = 3). All cells were transiently transfected with the RIG-I expression plasmid (10 ng).

B. Relative level of RIG-I signaling upon SeV infection (100 HA units/ml) in RIPLET$^{-/-}$ 293T cells complemented with empty vector (EV), RIPLET or ΔRING, as in (A).

C. dsRNA length-dependence of the effect of ΔRING on RIG-I signaling (mean ± s.d., $n$ = 3). Experiments were performed as in (A).

D. Effect of ΔRING and CC-swap mutants on RIG-I signaling in RIPLET$^{-/-}$ 293T upon stimulation with 162 bp dsRNA. Experiments were performed as in (A). On the right is the

WB of ΔRING and CC-swaps. Note that plasmids amount (100 ng for GST-PSpry and 20 ng for the rest) was adjusted to ensure comparable level of protein expression.

E. MAVS polymerization assay to examine the effect of ΔRING in the absence of K63-$Ub_n$. The RIG-I:dsRNA complex (1 μM RIG-I and 6 ng/μl 162 bp dsRNA) was incubated with an increasing concentration of ΔRING or GST-PSpry (0, 5, 12.5 μM), and mixed with purified monomeric MAVS CARD (10 μM). Polymerization of MAVS CARD was measured by native PAGE and EM. Right: representative images for MAVS CARD filaments nucleated with RIG-I filaments without ΔRING (*) or with ΔRING (**).

F. MAVS polymerization assay to examine the effect of ΔRING (12.5 μM) in the presence of an increasing concentration of K63-$Ub_n$ (equivalent to 0-7 μM monomeric Ub). Right: representative EM images of MAVS CARD filaments nucleated with RIG-I filaments without ΔRING (*) or with ΔRING (**), all in the presence of K63-$Ub_n$ (equivalent to 1.4 μM monomeric Ub).

G. A model of how RIPLET functions as a co-receptor for RIG-I. RIG-I first binds a dsRNA end as a monomer, but on long dsRNAs, it forms filamentous oligomers. RIPLET selectively binds filamentous RIG-I because bivalent binding is required for their high affinity interactions. On >~40 bp RNAs, RIPLET can also cross-bridge RIG-I filaments, leading to the higher-order receptor clustering and amplification of antiviral signaling. On much longer (>~1 kb) dsRNA, however, RIG-I inefficiently forms filaments (due to its assembly from dsRNA ends), which consequently limits RIPLET binding and antiviral signaling. Thus, RIPLET utilizes its ability to both recognize and alter the oligomerization state of RIG-I to differentially amplify antiviral signaling on the basis of the duplex RNA length.

## Materials & Methods

### Material Preparation

***Plasmids*** Mammalian and bacterial expression plasmids for RIG-I, MDA5 and MAVS and their truncation variants were described previously(*1, 2*). Human RIPLET, ΔRING (residues 94-433), ΔPSpry (residues 1-237) and PSpry (residues 249-433) were inserted between BamHI and EcoRI of pcDNA3-HA. GST-PSpry was generated first by inserting PSpry (residues 249-443) into pGEX6p-1 between BamHI and SalI. GST-PSpry in pGEX6p-1 was then amplified and inserted into pcDNA3-HA using the EcoRI site (for both 5' and 3' end restrictions). ΔRING was mutated into V127L (GTA→CTC) and T189E/S190F (ACTTCC→GAATTC) to engineer XhoI and EcoRI sites, respectively, and the sites were used to replace RIPLET CC by MCC and GCC (Fig. S4d). Note that V127L (GTA→CTC) and T189E/S190F (ACTTCC→GAATTC) alone did not impact the function of RIPLET. 4xFKBP-PSpry was generated by inserting four tandem repeats of FKBP (F36V variant, also known as DmrB) into the KpnI site in pcDNA3 containing PSpry between BamHI/EcoRI. Bacterial expression constructs for RIPLET, ΔRING and GCC-PSpry were generated using BamHI and SalI in pET47b. MCC-PSpry was cloned using BamHI and SalI in pET50b. GST-PSpry was expressed from pGEX6p-1. Human TRIM25 was cloned between EcoRI and XbaI in pcDNA3-HA vector (pcDNA3 with the HA-tag between KpnI and BamHI). Baculovirus expression construct for human TRIM25 was a generous gift from Owen Pornillos's lab. The bacterial expression construct for mouse E1 ubiquitin activating enzyme (pET28-mE1) was purchased from Addgene. Human Ubc13 and Uev1A were inserted between the XmaI and XhoI restriction sites in pET47b, and human ubiquitin (WT, K63R, K48R) were inserted between the XmaI and HindIII restriction sites in pET47b. Human ubiquitin (K63only) was purchased from AddGene and subcloned into pcDNA3 with the N-terminal His-tag. The

gene encoding residues 124 to 186 of RIPLET, corresponding to the coiled coil (CC) region, was inserted in pMAL-3C vector (pMAL where the cleavage site is inserted between KpnI and BamHI(*3*)) between BamHI and HindIII sites. A single Cys residue was incorporated at either end of the coiled coil, separated by a 4 residue linker (Gly-Ser-Gly-Ser), to generate two distinct forms of the construct namely Cys-GSGS-CC and CC-GSGS-Cys.

***Proteins*** Human RIG-I and MDA5 variants were expressed and purified as previously reported(*1, 4*). Briefly, the proteins were expressed in BL21(DE3) at 20˚C for 16-20 hr following induction with 0.5 mM IPTG. Cells were lysed by high pressure homogenization using an Emulsiflex C3 (Avestin), and the protein was purified by a combination of Ni-NTA and heparin affinity chromatography and size exclusion chromatography (SEC) in 20 mM Hepes, pH 7.5, 150 mM NaCl and 2 mM DTT. Human RIPLET and its variants were also expressed and purified in the same manner and purified by a combination of Ni-NTA and SEC. Human TRIM25 was expressed from SF9 insect cells and purified as previously described(*5*). Mouse E1, human Ubc13 and Uev1A and ubiquitins were prepared as previously reported(*1*).
For N-terminal fluorescent labeling of RIG-I and its variants, the protein (~2 mg/ml) was incubated with 0.5 mM peptide (LPETGG) conjugated with fluorescein (Anaspec) and 1.5 μM *S. aureus* sortase A (a gift from Hidde Ploegh, MIT)(*6*) at 4˚C for 4 hrs, followed by reverse Ni-NTA affinity purification and/or SEC to remove sortase.

MAVS CARD was expressed as a fusion protein with the SNAP tag in BL21(DE3) at 20˚C for 16-20 hr following induction with 0.4 mM IPTG. The SNAP tag allows fluorescent labeling of MAVS CARD. MAVS CARD-SNAP fusion was purified using Ni-NTA affinity chromatography and SEC as previously described(*7*), with the exception of using 0.05% NP-40

instead of CHAPS as a choice of detergent. Purified CARD-SNAP exists in the form of short filaments and was denatured in 6 M guanidinium hydrochloride for 30 min at 37˚C, followed by dialysis against 20 mM Tris, pH 7.5, 500 mM NaCl, 0.5 mM EDTA and 20 mM BME at 4˚C for 1 hr. Refolded CARD-SNAP was filtered using a 0.1μ filter and subsequently labeled with Alexa647-benzylguanine (NEB) on ice for 15 min according to the manufacturer's instruction, and was immediately used for filament formation assays.

Both RIPLET CC with Cys at the C-terminus (CC-GSGS-Cys) and N-terminus (Cys-GSGS-CC) were expressed and purified along with a cleavable 6xHis and MBP tag from *E. coli* BL21 (DE3) using Ni-NTA affinity chromatography followed by size exclusion chromatography in (50 mM Tris pH 7.5, 300 mM NaCl, 0.5 mM EDTA). The 6xHis and MBP tags were removed from both proteins using HRV 3C protease. CC-GSGS-Cys was subsequently fluorescently labeled by attaching FAM-conjugated peptide LPETGG (Anaspec) at the N-terminus using the protein ligase Sortase A. Purified CC-GSGS-Cys was incubated with *S. aureus* Sortase A in a molar ratio of 4:1 along with 0.5 mM FAM-LPETGG peptide for 6-8 hrs at RT in the dark followed by reverse Ni-NTA affinity chromatography to remove sortase.

***RNAs*** Double-stranded RNAs (dsRNAs) were prepared by *in vitro* T7 transcription as previously described(*8*). Unless mentioned otherwise, all dsRNAs contain 5'ppp and blunt end. The sequences of 28, 42, 62, 112, 162 and 512 RNAs were taken from the first 16, 30, 50, 100, 150 and 500 bp of the MDA5 gene flanked by 5'-gggaga and 5'-tctccc. The sequences of 15 bp and 21 bp dsRNAs are 5'-agggcccgggaugcu and 5'-gagucacgacguuguaaaaaa, respectively. The two complementary strands were co-transcribed, and the duplex was separated from unannealed ssRNAs by 15% acrylamide (15 and 21 bp), 8.5% acrylamide (28-162 bp) or 6% acrylamide

(512 bp) gel electrophoresis in TBE buffer. RNA was gel-extracted using the Elutrap electroelution kit (Whatman), ethanol precipitated, and stored in 20 mM Hepes, pH 7.0. Qualities of RNAs were analyzed by 1X TBE polyacrylamide gel.

For 3'-biotin labeling of RNA, the 3′ end of RNA was oxidized with 0.1 M sodium periodate in 0.25 M NaOAc, pH 5.5, at room temperature for 2 h. The reaction subsequently was treated with 0.2 M KCl, the buffer was replaced with 0.25 M NaOAc, pH 5.5, using Zeba desalting column (Pierce), and incubation EZ-Link Hydrazide-PEG4-Biotin (Pierce) continued at room temperature for 4–6 h. The labeled RNA was desalted twice to remove unincorporated biotin and was stored in 20 mM Hepes, pH 7.0, at -20 °C.

***Antibodies.*** For immuno-blotting, antibodies and their manufacturers were: Rabbit α-RIG-I (ENZO), rabbit α-HA (Cell Signaling), rabbit α-β-actin (Cells Signaling) mouse α-TRIM25 (BD), mouse α-Ub (Santa Cruz), α-RIPLET (in-house). For immunofluorescence, antibodies included: α-RIG-I (in-house)(*9*) and α-TIAR (Santa Cruz).

***IFNβ* promoter luciferase reporter assay**

HEK293T cells were maintained in 48-well plates in Dulbecco's modified Eagle medium (Cellgro) supplemented with 10% fetal calf serum and 1% penicillin/streptomycin. At ~80% confluence, cells were transfected with plasmids encoding RIG-I (10 ng), MDA5 (10 ng), MAVS (10 ng) or GST-2CARD (50 ng), together with the *IFNβ* promoter driven firefly luciferase reporter plasmid (100 ng) and a constitutively expressed Renilla luciferase reporter plasmid (pRL-CMV, 10 ng) by using lipofectamine 2000 (Life) according to the manufacturer's protocol. Empty vector was used to maintain the total amount of DNA and lipofectamine constant. In the experiments requiring RNA stimulation, the medium was changed 6hr after the first transfection

and the cells were additionally transfected with RNA (0.2 μg, Invivogen). Cells were lysed ~20 hrs post-stimulation and *IFNβ* promoter activity was measured using the Dual Luciferase Reporter assay (Promega) and a Synergy2 plate reader (BioTek). Firefly luciferase activity was normalized against Renilla luciferase activity.

**RT-qPCR**

HEK293T cells were stimulated with RNA in a similar manner as above. For SeV infection, cells were treated with SeV (100 HA units/ml, Charles River) with 1 hr of absorption. Cells were lysed ~20 hr post-infection. Total RNAs were extracted using TRIzol reagent (Thermo Fisher) and cDNA was synthesized using High Capacity cDNA reverse transcription kit (Applied Biosystems) according to the manufacture's instruction. Real-time PCR was performed using a SYBR Green Master Mix (Applied Biosystems), and the StepOne™ Real-Time PCR Systems (Applied Biosystems). *IFN-β* was amplified using primers GGGGCATGGAGAATAACTCA (forward) and AGCTGACACTTCCTTCTGCC (reverse). *GAPDH* was used as the internal normalization control and amplified using primers TGATGACATCAAGAAGGTGGTGAAG (forward) and TCCTTGGAGGCCATGTGGGCCAT (reverse).

**Ubiquitination reaction**

RIG-I ubiquitination was performed in the following manner. Purified RIG-I (1.0 μM) was first incubated with dsRNA (2 ng/μl) in buffer A (20 mM Hepes, pH 7.5, 150 mM NaCl, 1.5 mM $MgCl_2$, 2 mM ATP and 5 mM DTT) at RT for 15 min. The RIG-I:RNA complex (to the final RIG-I concentration of 0.5 μM) was then further incubated with 20 μM ubiquitin, 1 μM mE1, 5 μM Ubc13, 2.5 μM Uev1A and 0.25 μM E3 (RIPLET or TRIM25) in buffer B (50 mM Tris pH

7.5, 10 mM $MgCl_2$, 5 mM ATP and 0.6 mM DTT) at 37˚C for 30 min. For isoT treatment, isoT (10 ng/μl final) was added to the ubiquitination reaction, and further incubated at 37˚C for 30 min. Reactions were quenched with SDS loading buffer, boiled at 96 C for 5 min, and analyzed on SDS-PAGE by anti-RIG-I or anti-Ub western blot. Note that previous Ub-conjugation of RIG-I CARD by TRIM25(*10*) was performed with significantly higher protein concentrations, which explains the discrepancy with the current result in Fig. 1.

Unanchored K63-$Ub_n$ chains were generated from a reaction containing 0.4 mM ubiquitin, 4 μM mE1, 20 μM Ubc13 and 20 μM Uev1A in buffer B. The K63-$Ub_n$ synthesis reaction was performed overnight at 37˚C. Synthesized K63-$Ub_n$ chains were purified as described previously (*11*). Briefly, ubiquitin chains were diluted 5-fold into 50 mM ammonium acetate, pH 4.5, 0.1 M NaCl and separated over a 45 ml 0.1-0.6 M NaCl gradient in 50 mM ammonium acetate, pH 4.5 using a Hi-Trap SP FF column (GE Healthcare). High molecular weight fractions were applied to an S200 10/300 column equilibrated in 20 mM Hepes pH 7.5, 150 mM NaCl.

**MAVS polymerization assay**

The MAVS filament formation assay was performed as previously reported(*2*). Refolded, Alexa647 labeled monomer of CARD fused to SNAP (CARD-SNAP) was described in the material preparation section. In the absence of external stimuli or seed filaments, refolded MAVS CARD remains stably as a monomer over ~10-20 hr, after which it spontaneously forms prion-like filaments over the course of days. Thus, all assays involving MAVS filament formation were performed within 4 hr after refolding. To monitor stimulation of MAVS filament formation by RIG-I conjugated with ubiquitin chains, monomeric MAVS CARD-SNAP (10 μM) was incubated with conjugation reaction (to final RIG-I concentration of 1 μM) at RT for 1 hr prior to analysis by Bis-Tris native PAGE (Life) or by EM. Before running on the gel, all samples were subjected to

one round of freeze-thaw cycle by incubating on dry ice for 5 min followed by incubation at RT for 5 min. To examine the impact of ΔRING on MAVS stimulatory activity of RIG-I, RIG-I (1 μM) was pre-incubated with dsRNA (6 ng/μl) and 2 mM ATP in the presence or absence of K63-$Ub_n$ (equivalent to 0-7 μM monomeric Ub) in buffer A for 15 min at RT. This was followed by the addition of ΔRING (0, 5, 12.5 μM) and a further incubation at RT for 15 min. The mixture was then finally incubated with monomeric CARD-SNAP (10 μM) at RT for 1 hr prior to analysis by Bis-Tris native PAGE (Life) or by EM. Fluorescent gel images were recorded using an FLA9000 scanner (Fuji).

**Electron Microscopy**

RIG-I or RIG-IΔN (0.5 μM) was incubated with RNA (1 ng/μl) in buffer A at RT for 15 min followed by addition of RIPLET, ΔRING or its CC-swap variants (0.5 μM) and further incubated at RT for 15 min prior to EM grid preparation. Prepared samples were adsorbed to carbon-coated grids (Ted Pella) and stained with 0.75% uranyl formate as described(*12*). Images were collected using a Tecnai $G^2$ Spirit BioTWIN transmission electron microscope at 30,000x magnification for RIG-I filaments and 4,800x or 6,800x for MAVS filaments. Grids for the MAVS filaments were prepared and imaged as with the RIG-I filaments.

**Electrophoretic Mobility Shift Assay (EMSA)**

For RNA binding assays, dsRNA (1 ng/μl) was incubated with protein (at indicated concentration) in buffer A at RT for 10 min, and the complex was analyzed on Bis-Tris native PAGE (Life Technologies) after staining with SybrGold stain (Life Technologies). For RIG-I binding assays, fluorescein-labeled RIG-I was first incubated with dsRNA (1 ng/μl) and

subsequently with RIPLET (at indicated concentration) prior to analysis by Bis-Tris native PAGE (Life Technologies). SybrGold or fluorescein fluorescence was recorded using the scanner FLA9000 (Fuji) and analyzed with Multigauge (GE Healthcare).

**Streptavidin pull-down assay**

RIG-IΔN filaments (0.5 μM) were formed on non-biotinylated 162 bp dsRNA (1 ng/μl) and 3'-biotinylated 112 bp dsRNA (1 ng/μl), and were incubated with an increasing concentrations of ΔRING or GST-PSpry (0.25, 0.5, and 1μM) at RT for 15 min in buffer A. The reaction (250 μl) was further incubated with streptavidin-agarose (15 μl, NEB), washed three times with 0.5 ml buffer A, and eluted with 1 unit/ml protease K (NEB). Biotinylated 112 bp dsRNA was purified using streptavidin beads and co-purification of 162 bp dsRNA was analyzed on the 6% TBE gel. Gel image was taken using SybrGold stain fluorescence.

**Immunofluorescence imaging**

293T, HeLa and BMDM were infected with SeV or stimulated with 162 bp dsRNA with 5'ppp. 2 hr post RNA stimulation or 8 hrs (or 24 hrs) post-infection, cells were fixed with 2% paraformaldehyde at RT for 10 minutes, and permeabilized with 0.5% Triton-X at RT for 10 minutes. Cells were blocked for 30 min at RT with 1% BSA in PBST, and stained using RIG-I (1:100, in-house antibody) and TIAR (1:100, SC-398372) overnight. Images were obtained using a Zeiss Axio Imager M1 microscope at 100X magnification.

**Multi-Angle Light Scattering (MALS)**

The molecular masses of RIPLET, ΔRING and PSpry were determined by MALS using a Superose 200 10/300 column (GE) attached to a miniDAWN TRI-STAR detector (Wyatt Technology) in 20 mM Hepes, pH 7.5, 150 mM NaCl, 2 mM DTT and the data was analyzed using Astra V (Wyatt Technology).

**Coiled coil cross-linking assay**

The fluorescently labeled CC-GSGS-Cys (A* in Extended Data Fig. 4f) was mixed with equal molar amounts of unlabeled CC-GSGS-Cys (A) or Cys-GSGC-CC (B) in denaturation buffer (50 mM Tris 7.5, 300 mM NaCl, 0.5 mM EDTA, 20 mM BME, 6 M Urea) and incubated at 37°C for 30 min with constant shaking. The denatured protein mixtures were refolded by stepwise dilution into refolding buffer (denaturation buffer without Urea and BME). At each step, the mixture was diluted two-fold into refolding buffer and incubated at 4°C for 15 min with gentle rocking and the step repeated 4 times. Finally the refolded proteins were desalted into refolding buffer using 7K MWCO Zeba spin desalting columns (Thermo Fisher Scientific).

The refolded protein dimers were cross-linked by incubating with 100 μM crosslinker bismaleimidoethane (BMOE) or m-maleimidobenzoyl-N-hydroxysulfosuccinimide ester (Sulfo-MBS) (Thermo Fisher Scientific) at RT for 10 min. The cross-linked dimers were run on a 20% SDS-PAGE and scanned for FAM fluorescence using FLA9000 scanner (Fuji).

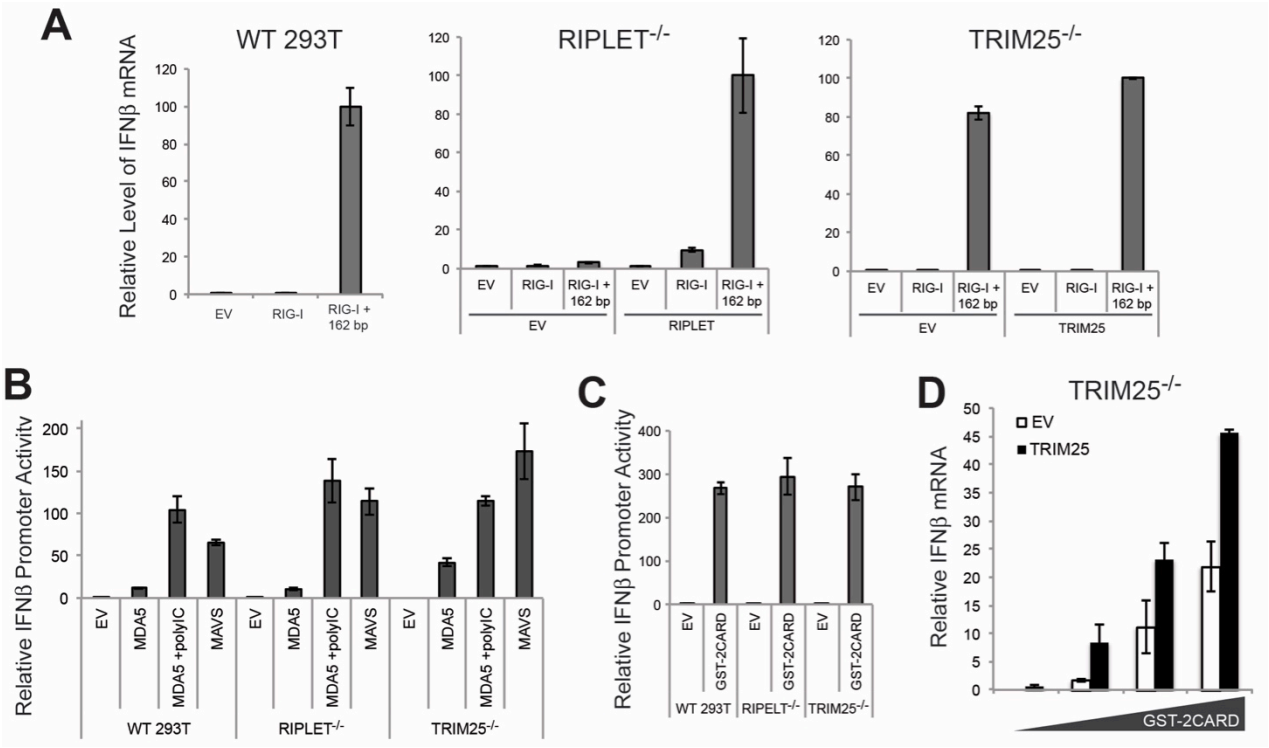


**Supplementary Fig. 1 RIPLET, not TRIM25, is required for RIG-I signal activation.**

A. Relative level of RIG-I signaling upon stimulation with dsRNA, as measured by the IFNβ mRNA level (mean ± s.d., $n$ = 3). 293T cells (WT, RIPLET$^{-/-}$ or TRIM25$^{-/-}$) were transfected with empty vector (EV) or the RIG-I expression plasmid (10 ng), and stimulated with 162 bp dsRNA with 5'ppp (0.2 μg). In RIPLET$^{-/-}$ and TRIM25$^{-/-}$ cells, additional plasmid expressing RIPLET or TRIM25 (10 ng) was co-transfected with RIG-I to test complementation.

B. Relative signaling activities of MDA5 (10 ng) and MAVS (50 ng) in 293T cells (WT, RIPLET$^{-/-}$ or TRIM25$^{-/-}$), as measured by the IFNβ promoter reporter assay (mean ± s.d., $n$ = 3). MDA5 was stimulated with high molecular weight polyinosinic-polycytidylic acid (polyIC, 0.2 μg).

C. Relative signaling activity of RIG-I 2CARD fused to GST (GST-2CARD) (10 ng) in 293T cells (WT, RIPLET$^{-/-}$ or TRIM25$^{-/-}$), as measured by the IFNβ promoter reporter assay (mean ± s.d., $n$ = 3). Note that antiviral signaling by GST-2CARD occurs in a RIPLET-independent manner because, as shown in Fig. 2a, RIPLET does not recognize the isolated 2CARD. The RIPLET-independent signaling activity of GST-2CARD may reflect the potential ability of dimeric GST to promote 2CARD tetramerization in the absence of K63-Ub$_n$.

D. Relative signaling activity of GST-2CARD in TRIM25$^{-/-}$ 293T cells in the presence or absence of ectopically expressed TRIM25. An increasing amount of GST-2CARD expression construct (0, 10, 50 and 100 ng) was co-transfected with TRIM25 expression construct or empty vector (EV) (10 ng). The signaling activity of GST-2CARD was measured by the IFNβ mRNA level (mean ± s.d., $n$ = 3). While knocking out TRIM25 had little impact on GST-2CARD signaling in (c), ectopic expression of TRIM25 increases antiviral signaling, as previously reported(*13*).

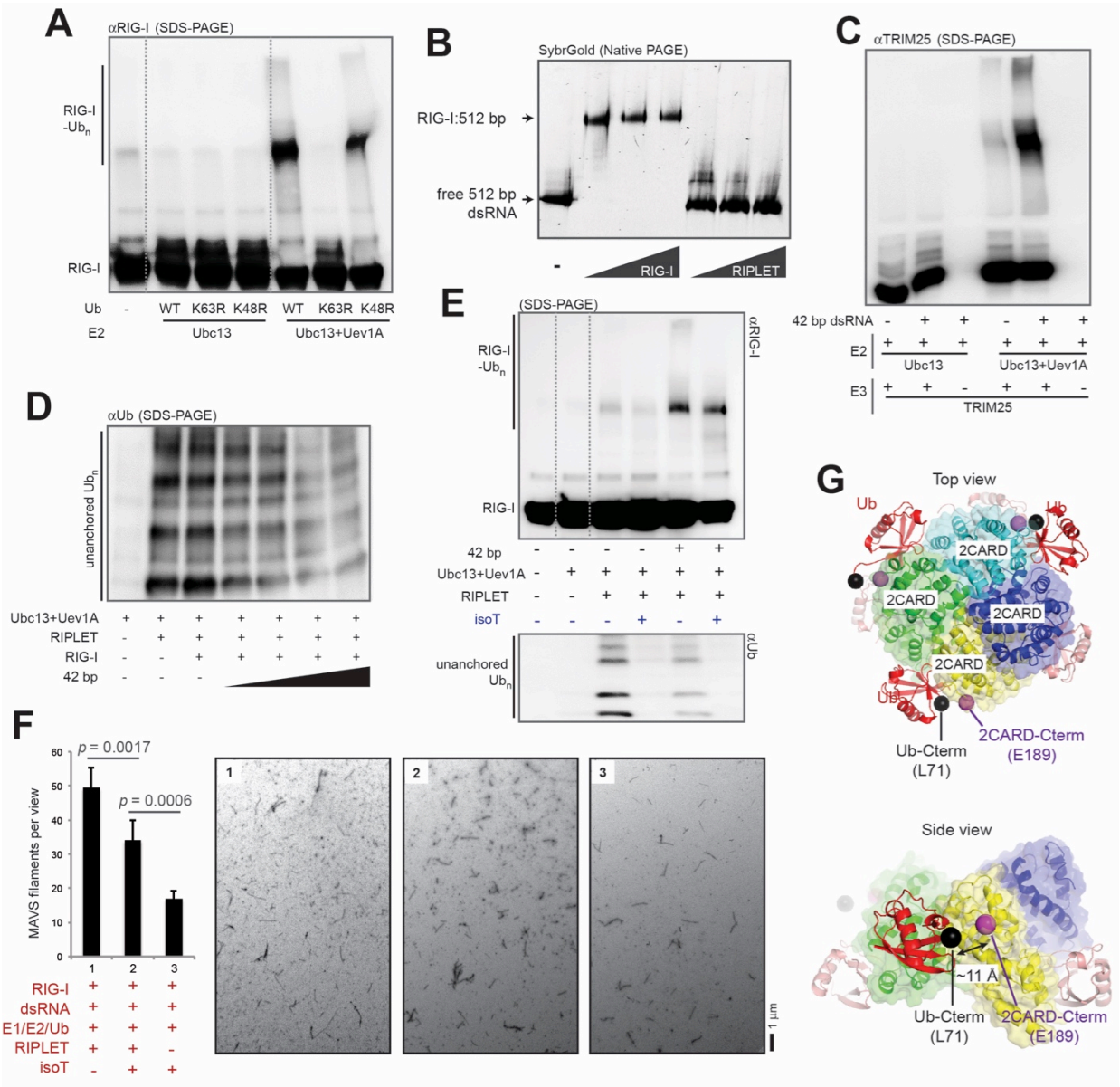


**Supplementary Fig. 2 RIPLET, not TRIM25, ubiquitinates RIG-I in a dsRNA-dependent manner.**

A. *In vitro* ubiquitination analysis of RIG-I. Purified E1, E2 (Ubc13 alone or in complex with Uev1A), E3 (RIPLET) and Ub (WT, K63R or K48R) were incubated with RIG-I. Ubiquitination of RIG-I was analyzed by anti-RIG-I blot on a SDS gel, all in the presence of 42 bp dsRNA. Experiments were performed as in Fig. 1c. While mono- or di-Ub adducts were found with Ubc13 alone, long Ub chain adduct was formed only with the Ubc13:Uev1A complex. The K63R mutation in Ub abolished long Ub chain adduct formation, suggesting that RIPLET (together with Ubc13:Uev1A) conjugates K63-linked $Ub_n$ chains to RIG-I.

B. RNA binding of RIG-I and RIPLET, as measured by native gel shift assay. An increasing concentration of RIG-I and RIPLET (0.25, 0.5, 1 μM) was used. Gel image was obtained using fluorescence of RNA stained with SybrGold.
C. *In vitro* auto-ubiquitination analysis of TRIM25. Samples with TRIM25 in Fig. 1c were re-analyzed by anti-TRIM25 blot.
D. *In vitro* synthesis of unanchored Ub chains by RIPLET, with and without RIG-I or 42 bp dsRNA (1-4 ng/μl). The reaction was performed as in Fig. 1c, and analyzed by anti-Ub blot. Only the low molecular weight species (<~50 kDa) are shown to avoid detection of RIG-I-conjugated Ub, which would be > ~100 kDa.
E. Sensitivity of anchored and unanchored Ub chains to the isoT peptidase. The ubiquitination reaction was performed as in Fig. 1c for 30 min at 37˚C, and further incubated with isoT (10 ng/μl) for 30 min at 37˚C, prior to gel analysis. Anchored and unanchored Ub chains were analyzed by anti-RIG-I and anti-Ub blotting, respectively. The result showed that while unanchored Ub chains were completely degraded by isoT (in line with its known substrate specificity), RIG-I-anchored Ub chains were also degraded, albeit at a lower efficiency.
F. EM analysis of MAVS CARD filaments induced by RIG-I after ubiquitination with RIPLET and/or treatment with isoT. Based on six random images collected at 6,800x magnification (right), average number (± s.d.) of MAVS filaments per image was plotted. RIG-I-induced MAVS stimulation is most efficient after the RIPLET reaction before isoT treatment (sample 1). IsoT somewhat reduces the MAVS stimulatory activity (sample 2), but is still more efficient than without RIPLET (sample 3). The moderate effect of isoT could be due to partial degradation of anchored Ub chains and/or complete degradation of unanchored Ub chains (see (e)).
G. The crystal structure of the 2CARD tetramer in complex with K63-$Ub_2$, from the top view (left) and side view (right) (PDB:4NQK)(*10*). The most C-terminal residues in individual 2CARD subunits and Ub molecules are indicated by purple and black spheres, respectively. The structure showed that the C-terminal region of RIG-I 2CARD (residues ~190-200) is flexible and is located in close proximity to the Ub binding site. Our mass spectrometric analysis of ubiquitinated RIG-I showed that K190 and K193, residing within this flexible 2CARD tail, are ubiquitinated by RIPLET. Based on the structure, one could predict that K63-$Ub_n$ covalently conjugated to K190 or K193 would bind 2CARD and stabilize the tetramer as in the crystal structure. Note that mass spectrometry identified additional Ub conjugation sites, such as K925 (at the C-terminus) and K666 (within the helicase loop), suggesting that RIPLET can modify multiple flexible regions in RIG-I.

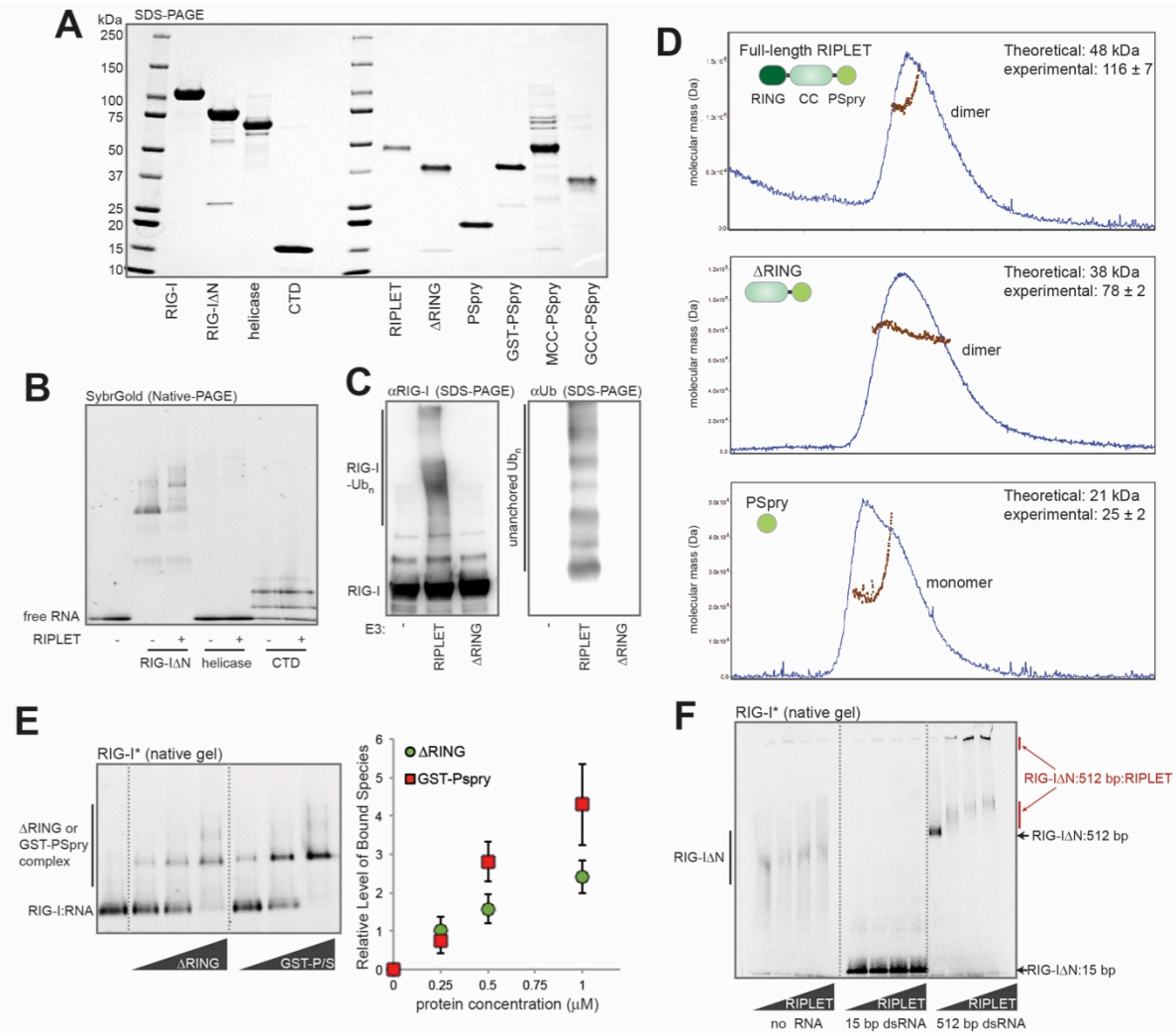


**Supplementary Fig. 3 RIPLET utilizes bivalency to selectively recognize RIG-I on pre-oligomerized dsRNA.**

A. SDS-PAGE analysis of purified RIG-I and RIPLET variants used in this study.

B. Native gel shift assay of RIG-I variants with RIPLET. 42 bp dsRNA (1 ng/μl) was incubated with RIG-IΔN, the helicase domain or CTD (0.5 μM), in the presence or absence of RIPLET (0.5 μM). Electrophoretic mobility of 42 bp dsRNA was measured using fluorescence of SybrGold stain. The helicase domain has only a weak affinity to dsRNA. Neither the helicase domain nor CTD display mobility shift upon RIPLET addition.

C. *In vitro* Ub chain synthesis by RIPLET or ΔRING. Both RIG-I-anchored Ub (left) and unanchored Ub (right) were analyzed with RIPLET and ΔRING. Left: the ubiquitination reaction was performed in the presence of 42 bp dsRNA (as in Fig. 1c), and anchored Ub chains was analyzed by anti-RIG-I blot. Right: the ubiquitination reaction was performed without RIG-I or 42 bp dsRNA (as they are unnecessary for unanchored Ub synthesis, Extended Data Fig. 2d) and was analyzed by anti-Ub blot. Note that the two blots cover different molecular weight ranges; the anti-RIG-I blot is for >~100 kDa, whereas the anti-Ub blot is for <~50 kDa.

D. Multi-angle light scattering (MALS) traces of full-length RIPLET, ΔRING and PSpry. Theoretical and experimental molecular weights are shown on the upper right corner. Only PSpry exists as a monomer, while full-length RIPLET and ΔRING are constitutive dimers. Blue and brown traces indicate $OD_{280}$ and estimated molecular weight, respectively.
E. Native gel shift assay to compare the RIG-I binding efficiency of ΔRING and GST-PSpry. Right: quantitation of the bound species (mean ± s.d., $n = 3$).
F. Native gel shift assay to monitor RIG-I:RIPLET interaction. Fluorescently labeled RIG-IΔN (300 nM) was incubated with RIPLET (0, 150, 300, 600 nM) in the presence or absence of 15 bp or 512 bp dsRNA (2.5 ng/μl), and the complex was analyzed by native gel using RIG-I fluorescence. Note that there are two populations of the RIG-I:512 bp:RIPLET complex, one migrating into the gel and the other remaining in the gel well.

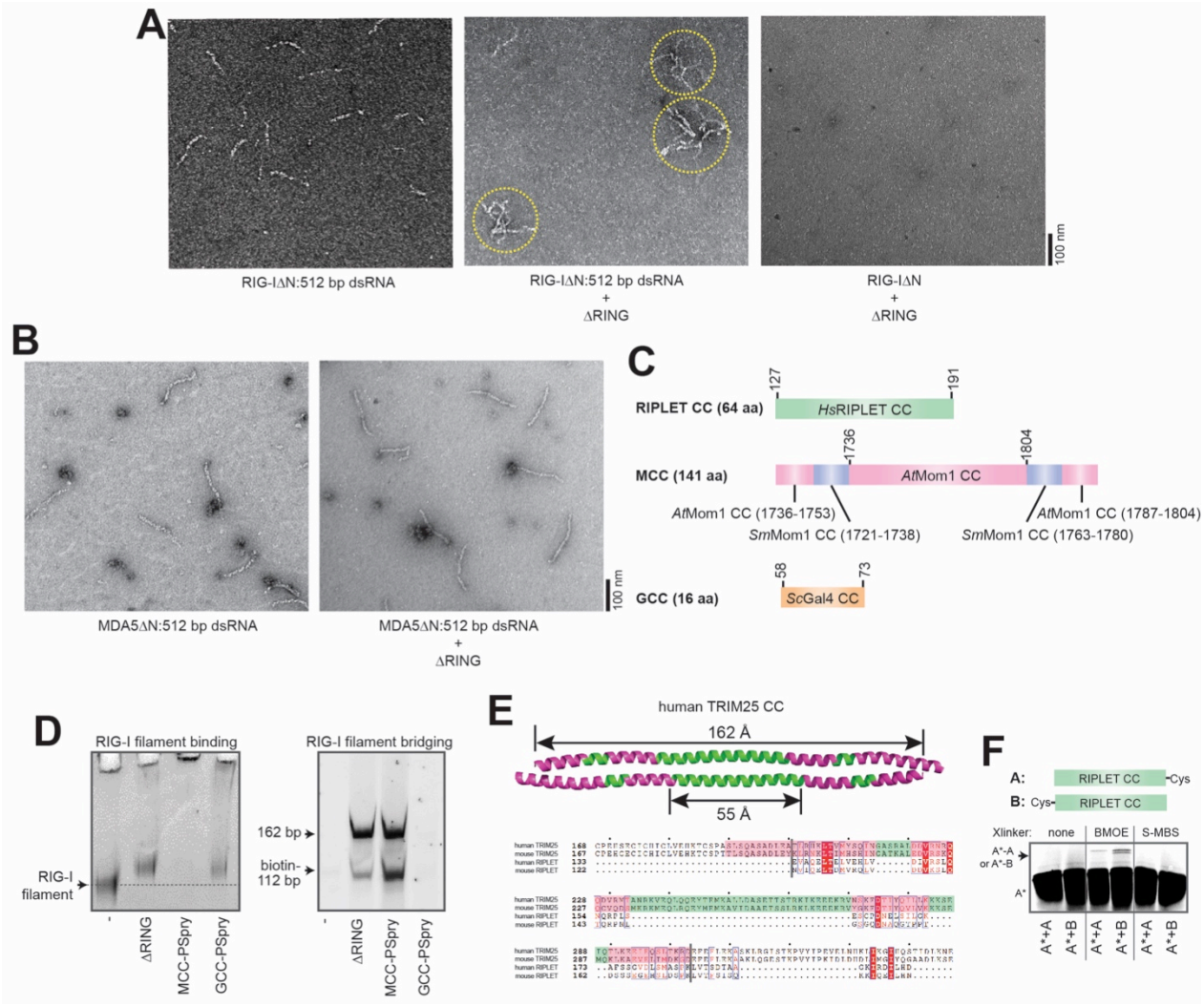


**Supplementary Fig. 4 RIPLET cross-bridges RIG-I filaments in an Ub-independent manner.**

A. Representative EM images of RIG-IΔN filaments (0.5 μM) formed on 512 bp dsRNA (1 ng/μl), in the presence and absence of ΔRING (0.5 μM). RIG-IΔN with ΔRING without 512 bp dsRNA is also shown on the right. Cross-bridged RIG-I filaments are highlighted with yellow circles.

B. Representative EM images of MDA5ΔN filaments (0.4 μM) formed on 512 bp dsRNA (1 ng/μl), in the presence and absence of ΔRING (0.4 μM). Due to the instability of the MDA5 filament on EM grids, ADP•$AlF_4$ (1 mM) was added prior to the grid preparation. Previous EM analysis of MDA5 filaments similarly required ADP•$AlF_4$ to stabilize the filament on the grid(*2, 8*).

C. Schematic of coiled coils (CCs) used in this study. *Homo sapiens* RIPLET CC (*Hs*RIPLET CC) indicates residues 127-191. *Saccharomyces cerevisiae* Gal4 CC (*Sc*GCC) indicates residues 58-73. Mom1 CC (MCC) was generated by symmetrically extending *Arabidopsis thaliana* Mom1 CC (*At*Mom1, residues 1736-1804)(*14*) with parts of *At*Mom1 CC and *Selaginella moellendorffii* MOM CC (*Sm*Mom1 CC) to generate 141 amino acid-long antiparallel CC.

D. Comparison of CC variants of RIPLET in terms of RIG-I filament binding and cross-bridging activities. Left: Native gel shift assay showing that RIG-IΔN filament (0.5 μM) on 512 bp dsRNA (1 ng/μl) is efficiently bound by ΔRING, MCC-PSpry and GCC-PSpry (0.5 μM for all). Note that RIG-IΔN filament in complex with MCC-PSpry does not enter the gel. Right: Streptavidin pull-down analysis to examine RIG-I filament cross-bridging by ΔRING, MCC-PSpry and GCC-PSpry. The experiment was performed as in Fig. 3c. The result shows that ΔRING and MCC-PSpry can cross-bridge RIG-I filaments, while GCC-PSpry cannot. Note that even the biotinylated 112 bp dsRNA is inefficiently purified with GCC-PSpry or without any RIPLET variants, suggesting that biotinylated 112 bp dsRNA is also purified largely through the filament cross-bridging mechanism, rather than through direct binding to the streptavidin beads.

E. Sequence analysis of the RIPLET coiled coil (CC) domain. NCBI Blast analysis of RIPLET identifies TRIM25 as the most closely related protein (sequence identity 32%, and 61% homology) among the human genes (UniProt database). Bottom: Sequence alignment of RIPLET CC and TRIM25 CC using Clustal Omega (EMBL-EBI). Top: The structure of TRIM25 CC (PDB code: 4LTB)(*15*). As with other members of the TRIM family characterized to date(*15, 16*), TRIM25 CC displays the antiparallel dimeric geometry. The TRIM25 CC was colored according to its sequence homology to RIPLET CC (green and magenta for aligned and non-aligned regions, respectively). The symmetric arrangement of the homologous regions suggests that RIPLET CC is also likely to be antiparallel. This notion was further supported by the cross-linking analysis in (f).

F. Cys-Cys crosslinking to distinguish between parallel and antiparallel CC geometries. RIPLET CC with Cys at either the C-terminus (A) or N-terminus (B) was purified as a homo-dimer. CC(A) was N-terminally labeled with fluorescein (A*) and denatured and refolded with an equimolar amount of unlabeled CC(A) or CC(B). The refolded dimer was cross-linked using a Cys-Cys specific crosslinker, BMOE (100 μM), or a Cys-Lys specific crosslinker, S-MBS (100 μM, control). Dimer cross-linking was analyzed by SDS-PAGE using fluorescein fluorescence. The more prominent crosslinking between A* and B than between A* and A suggests that RIPLET CC is likely an antiparallel dimer.

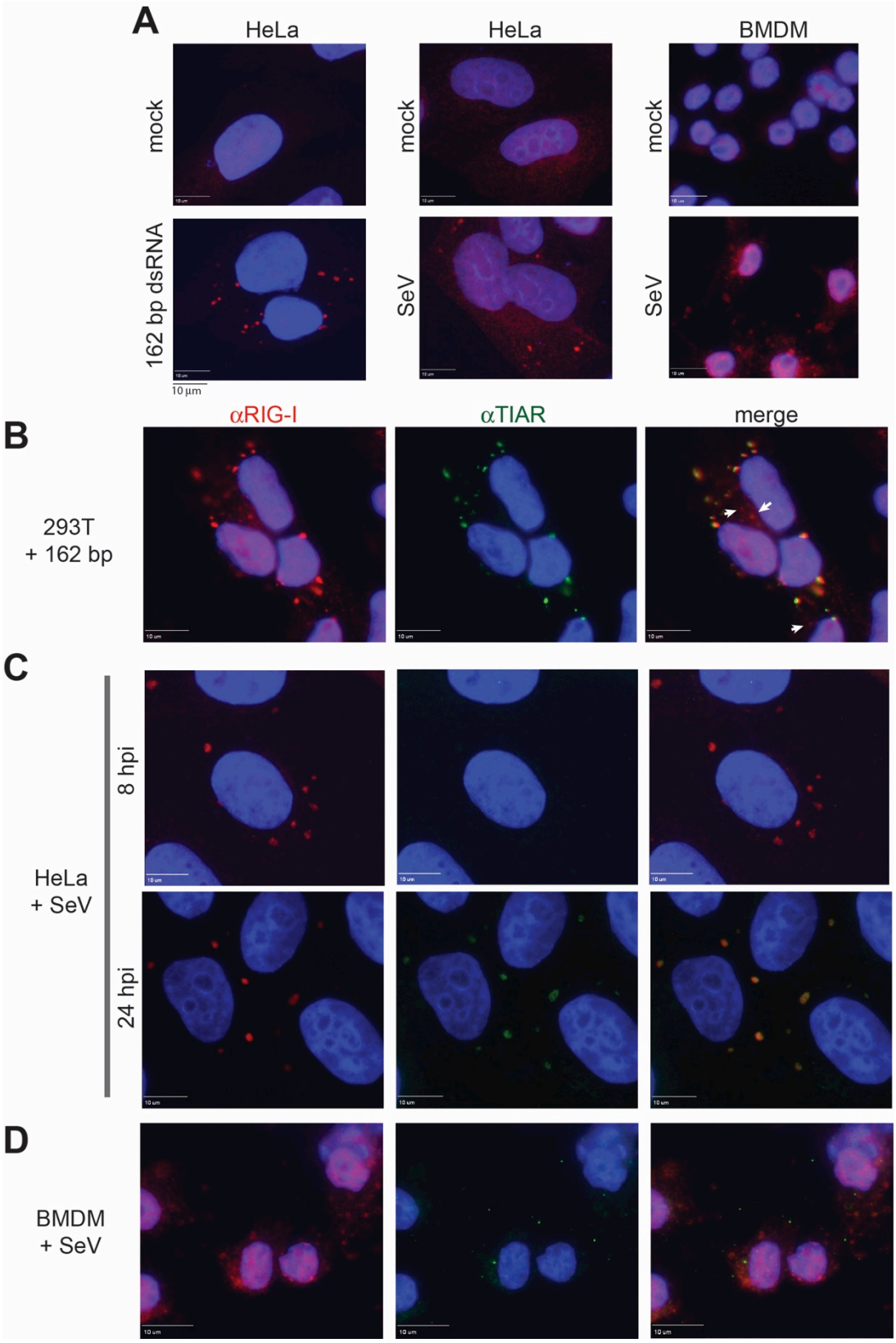
A
HeLa
HeLa
BMDM
mock
mock
mock
162 bp dsRNA
SeV
SeV
10 µm
B
αRIG-I
αTIAR
merge
293T
+ 162 bp
C
8 hpi
24 hpi
HeLa
+ SeV
D
BMDM
+ SeV

**Supplementary Fig. 5 RIPLET promotes RIG-I granule assembly upon viral infection or RNA stimulation.**

A. Immunofluorescence analysis of endogenous RIG-I granules (red) in HeLa cells or bone-marrow-derived mouse macrophages (BMDM) upon stimulation with 162 bp dsRNA or SeV infection. Cells were fixed 2 hr post RNA stimulation or 8 hr post SeV infection. DAPI staining (blue) indicates the nucleus.

B-D. Immunofluorescence analysis of endogenous RIG-I granules (red) and stress granules (αTIAR, green) in (b) 293T, (c) HeLa, and (d) BMDM. (b) 293T cells were transfected with 162 bp dsRNA and stained with αRIG-I and αTIAR 2 hr post-transfection. RIG-I granules partially co-localize with stress granules. Arrows indicate RIG-I granules not co-localized with stress granules. (c-d) HeLa cells and BMDM were infected with SeV (100 HA units/ml), and imaged 8 hr or 24 hr post-infection (hpi) for HeLa and 8 hr hpi for BMDM. Note that RIG-I granules at 8 hpi do not co-localize with stress granules in either HeLa or macrophages, while they do at 24 hpi in HeLa.

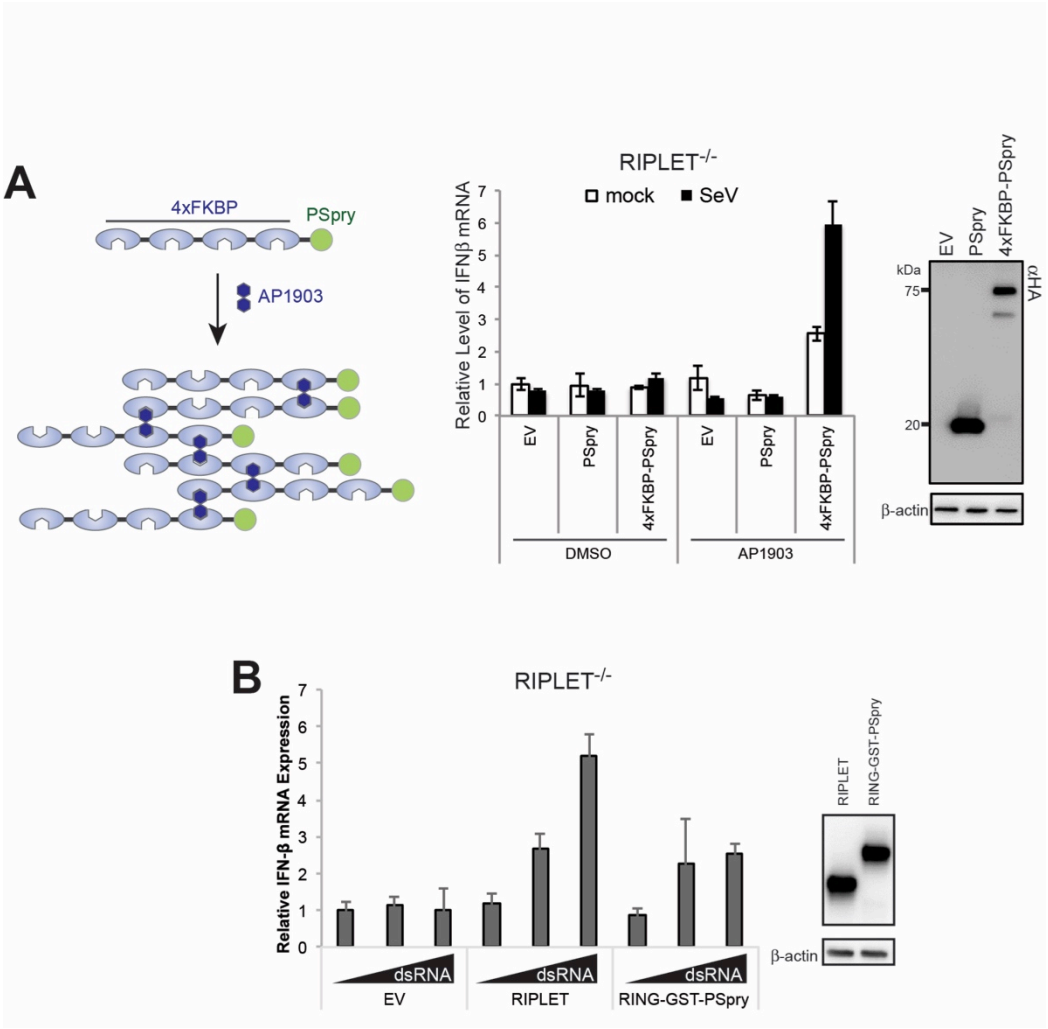


**Supplementary Fig. 6 RIPLET-mediated RIG-I aggregation enhances antiviral signaling, both in ubiquitin-dependent and -independent manners.**

A. Relative level of RIG-I signaling upon stimulation with SeV, as measured by the IFNβ mRNA level (mean ± s.d., $n = 3$). Left: schematic of oligomerization of 4xFKBP-PSpry in the presence of AP1903. Center: RIPLET$^{-/-}$ 293T cells were co-transfected with plasmids expressing RIG-I (10 ng) and 4xFKBP-PSpry (200 ng), and infected with SeV (100 HA units/ml) in the presence or absence of 2 μM AP1903. Since efficient introduction of AP1903 requires low (1%) serum medium, which alone increases the basal level of IFNβ over time, we analyzed IFNβ induction 6 hr post-infection (hpi), instead of 24 hr (as in other experiments in this study). While IFNβ induction at 6 hpi is lower than at 24 hpi, AP1910-dependent stimulation of RIG-I signaling was still evident in the presence of 4xFKBP-PSpry, but not with PSpry. Right: anti HA-western blot of PSpry and 4xFKBP-PSpry.

B. Comparison of full-length RIPLET vs. RING fused to GST-PSpry (RING-GST-PSpry) (20 ng each) in the RIG-I stimulatory activity. Left: Relative level of endogenous RIG-I signaling was measured upon stimulation with 162 bp dsRNA (0.2 μg) in RIPLET$^{-/-}$ 293T (mean ± s.d., $n = 3$). Right: anti HA-western blot of RIPLET or RING-GST-PSpry.

**References for Supplementary Data**


1. A. Peisley, B. Wu, H. Yao, T. Walz, S. Hur, RIG-I Forms Signaling-Competent Filaments in an ATP-Dependent, Ubiquitin-Independent Manner. *Mol Cell* **51**, 573-583 (2013).
2. B. Wu *et al.*, Structural Basis for dsRNA Recognition, Filament Formation, and Antiviral Signal Activation by MDA5. *Cell* **152**, 276-289 (2013).
3. A. Alexandrov, K. Dutta, S. M. Pascal, MBP Fusion Protein with a Viral Protease Cleavage Site: One-Step Cleavage/Purification of Insoluble Proteins. *BioTechniques* **30**, 1194-1198 (2001).
4. S. Ahmad *et al.*, Breaching self-tolerance to Alu duplex RNA underlies MDA5-mediated inflammation *Cell* **172**, 797-810 (2018).
5. J. G. Sanchez *et al.*, Mechanism of TRIM25 Catalytic Activation in the Antiviral RIG-I Pathway. *Cell Rep* **16**, 1315-1325 (2016).
6. J. M. Antos *et al.*, Site-specific N- and C-terminal labeling of a single polypeptide using sortase of different specificity. *J. Am. Chem. Soc.* **131**, 10800-10801 (2009).
7. B. Wu, Y. S. Huoh, S. Hur, Measuring Monomer-to-Filament Transition of MAVS as an In Vitro Activity Assay for RIG-I-Like Receptors. *Methods Mol Biol* **1390**, 131-142 (2016).
8. A. Peisley *et al.*, Cooperative Assembly and Dynamic Disassembly of MDA5 Filaments for Viral dsRNA Recognition. *Proc Natl Acad Sci U S A* **108**, 21010-21015 (2011).
9. S. W. Oh *et al.*, Leader-Containing Uncapped Viral Transcript Activates RIG-I in Antiviral Stress Granules. *PLoS Pathog* **12**, e1005444 (2016).
10. A. Peisley, B. Wu, H. Xu, Z. J. Chen, S. Hur, Structural basis for ubiquitin-mediated antiviral signal activation by RIG-I. *Nature* **509**, 110-114 (2014).
11. K. C. Dong *et al.*, Preparation of distinct ubiquitin chain reagents of high purity and yield. *Structure* **19**, 1053-1063 (2011).
12. M. Ohi, Y. Li, Y. Cheng, T. Walz, Negative staining and image classification - powerful tools in modern electron microscopy. *Biol. Proced. Online* **6**, 23-34 (2004).
13. M. U. Gack *et al.*, TRIM25 RING-finger E3 ubiquitin ligase is essential for RIG-I-mediated antiviral activity. *Nature* **446**, 916-920 (2007).
14. T. Nishimura *et al.*, Structural basis of transcriptional gene silencing mediated by Arabidopsis MOM1. *PLoS Genet* **8**, e1002484 (2012).
15. J. G. Sanchez *et al.*, The tripartite motif coiled-coil is an elongated antiparallel hairpin dimer. *Proc Natl Acad Sci U S A* **111**, 2494-2499 (2014).
16. C. Weinert, D. Morger, A. Djekic, M. G. Grutter, P. R. Mittl, Crystal structure of TRIM20 C-terminal coiled-coil/B30.2 fragment: implications for the recognition of higher order oligomers. *Sci Rep* **5**, 10819 (2015).